Am J Cancer Res 2025;15(5):2301-2318
www.ajcr.us /ISSN:2156-6976/ajcr0160290

Original Article

The role of LRRC15-SCG5 in ECM protein binding as a prognostic signature for urothelial carcinoma

Shao-Wei Dong[1,2*], Chih-Heng Chen[1,2*], Kai-Yi Tzou[1,2,3], Su-Wei Hu[1,2], Chia-Chang Wu[1,2,3], Chien Hsiu Li[1]

[1]Department of Urology, Shuang Ho Hospital, Taipei Medical University, New Taipei, Taiwan; [2]Taipei Medical University (TMU) Research Center of Urology and Kidney, Taipei Medical University, Taipei, Taiwan; [3]Department of Urology, School of Medicine, College of Medicine, Taipei Medical University, Taipei, Taiwan. [*]Equal contributors.

Received September 2, 2024; Accepted May 18, 2025; Epub May 25, 2025; Published May 30, 2025

Abstract: Membrane-bound LRRC15 facilitates communication with adjacent cells by interacting with extracellular molecules, yet its role in urothelial carcinoma remains undefined. A systematic analysis of clinicopathological transcriptome profiles of urothelial carcinoma patients reveals that dysregulated levels of LRRC15 are associated with tumor malignancy features and poor prognosis. A clinically based molecular simulation model highlights potential mechanisms whereby LRRC15 mediates urothelial carcinoma cell motility and growth, primarily through the extracellular matrix organization pathway. Further molecular interaction mapping identifies SCG5 as a novel molecule linking to LRRC15 via protein-protein interactions, positively correlating with advanced pathological features and worse prognosis in urothelial carcinoma patients. Kaplan-Meier plotter results indicate that the LRRC15/SCG5 axis can serve as a prognostic marker for low survival rates in both non-muscle invasive and muscle-invasive bladder cancer. Molecules affected by the LRRC15/SCG5 axis in bladder cancer and upper tract urothelial carcinoma contribute to signatures of poor prognosis in urothelial carcinoma. These findings support targeting the LRRC15/SCG5 axis as a potential therapeutic strategy to intervene in urothelial carcinoma progression.

Keywords: LRRC15, SCG5, bladder cancer, bioinformatics, extracellular matrix protein

Introduction

According to the American Cancer Society, there were 83,190 new cases of urinary bladder-related tumors and approximately 16,840 deaths in 2024. This high incidence and mortality rate place bladder cancer among the top ten most concerning cancer types, underscoring the urgent need for novel diagnostic strategies to intervene in tumor progression [1]. The five-year survival rate for patients diagnosed with metastatic events plummets from approximately 80% to 5% [2]. The genomic heterogeneity of urothelial carcinoma, compounded by its origin in both the upper tract and bladder tissues, adds to its complexity [3]. Various carcinogens, including tobacco exposure, have been implicated in the development of urothelial carcinoma and subsequent bladder cancer [2, 4-7]. Pathologically, bladder cancer is categorized based on the extent of muscle invasion in the bladder wall into non-muscle invasive bladder cancer (NMIBC) and muscle invasive bladder cancer (MIBC). While nearly 70% of superficial tumors can be managed initially through Transurethral Resection of Bladder Tumor (TURBT), the recurrence rate exceeds 50% [8-10]. Despite genomic differences, about half of MIBC cases are believed to originate from recurrent NMIBC [11, 12]. Furthermore, approximately 50% of MIBC patients experience metastasis even after undergoing neoadjuvant chemotherapy and cystectomy [11, 13]. Therefore, there is an urgent need to develop enhanced diagnostic strategies and tools for urothelial carcinoma, including prognostic biomarkers.

Leucine-rich repeat containing 15 (LRRC15) is a member of the Leucine-rich repeat-containing (LRRC) protein family, distinguished by its Leucine-rich repeat (LRR) domains. Notably, the LRR structure functions as a receptor for recognizing non-mammalian pathogens, including

https://doi.org/10.62347/ABZG4705

toll-like and NOD-like receptors [14]. Sequence alignment with the coxsackievirus-adenovirus receptor indicates that LRRC15 influences cellular susceptibility to adenovirus infections [15]. Dysregulated expression of LRRC15 has been identified as a prognostic factor in glioblastoma, ovarian cancer, osteosarcoma, and breast cancer [16-21]. LRRC15, a transmembrane protein, is considered an adhesion protein antigen due to its interactions with extracellular molecules [15, 22, 23]. In ovarian cancer, the interaction between LRRC15 and integrin promotes tumor motility and metastasis [24]. Upregulated LRRC15 has also been implicated in drug resistance in osteosarcoma and prostate cancer [25, 26]. The expression of LRRC15 is transactivated by TGF-β, particularly in activated mesenchymal-like tissues such as corneal and periodontal ligament cells [27, 28]. In tumor biology, upregulated LRRC15, regulated by TGF-β in tumor-associated fibroblasts [29, 30], alters invasive activity and enhances immune evasion of cancer cells [29-32]. However, no studies have comprehensively addressed the clinicopathological significance and potential molecular mechanisms of LRRC15 as a prognostic marker in urothelial carcinoma.

By re-analyzing the TCGA-BLCA transcriptome profiles, this study reveals for the first time the distribution of LRRC15 in tumors and its correlation with different pathological features and prognostic values. A molecular simulation model identified SCG5 as a potential protein partner of LRRC15, involved in LRRC15-mediated urothelial carcinoma malignancy. This systematic analysis indicates that dissecting the LRRC15/SCG5 axis and its downstream effectors can enhance therapeutic strategies for intervening in urothelial carcinoma.

Results

Elevated LRRC15 is a marker of malignancy in urothelial carcinoma patients

To confirm the association between elevated LRRC15 levels and high-risk cancer incidence, a pan-cancer analysis was conducted. Hazard ratio values indicated that LRRC15 distribution is linked to high-risk events across various cancer types, including urothelial carcinoma (**Figure 1A**). A volcano plot comparing TCGA (The Cancer Genome Atlas Program) transcriptome profiles between pathological stage I and stage IV revealed increased LRRC15 levels in advanced stage IV BLCA patients compared to early stage I, supporting the hypothesis that LRRC15 is associated with malignancy features and contributes to high-risk incidence in BLCA (**Figure 1B**; Supplementary Table 1). Specifically, compared to adjacent normal tissues, LRRC15 was significantly upregulated in urothelial carcinoma tissues in TCGA-BLCA patients ($P < 0.002004$) (**Figure 1C**; Supplementary Table 2). Similar results were observed in paired adjacent normal and tumor tissues from the same patients, showing a significant increase in LRRC15 in urothelial carcinoma ($P = 0.0004$) (**Figure 1D**). Interestingly, high levels of LRRC15 in tumor tissues were more pronounced in female patients compared to male patients ($P = 0.0103$) (**Figure 1E**; Supplementary Table 1). Consistent with the volcano plot, upregulated LRRC15 levels were observed in advanced BLCA patients defined as pathological stage III and IV compared to stage I and II ($P < 0.0001$) (**Figure 1F**). In pathological T events, high LRRC15 levels were observed in advanced pathological T3+T4 compared to T1+T2 ($P < 0.0001$) (**Figure 1G**). Similarly, in pathological N, patients with lymph node metastasis had significantly higher LRRC15 levels compared to those without lymph node metastasis ($P = 0.0009$) (**Figure 1H**). Notably, increased LRRC15 levels were significantly observed in tissues with lymph node metastasis only ($P = 0.0012$) (**Figure 1I**). Currently, exposure to risk factors like tobacco is recognized as contributing to bladder cancer progression [33]. TCGA-BLCA transcriptome profiles revealed that LRRC15 levels increased with the duration of tobacco smoking history, suggesting that repeated tobacco exposure may stimulate LRRC15 upregulation (**Figure 1J**). Further analysis of overall survival based on LRRC15 levels in patients' tissues showed that high LRRC15 levels are associated with worse prognosis in the TCGA-BLCA cohort ($P = 0.0232$ [HR = 1.406 (1.048-1.887)]) (**Figure 1K**; Supplementary Table 3). Similarly, analysis of the GSE13507 bladder cohort, which differentiates non-muscle invasive (NMIBC) and muscle invasive (MIBC) bladder cancer, indicated that patients with high LRRC15 transcript levels had poorer overall survival outcomes (NMIBC: $P = 0.0369$ [HR = 2.108 (1.046-4.248)], MIBC: $P = 0.0206$ [HR = 2.768 (1.169-6.554)]). The *P*-values and

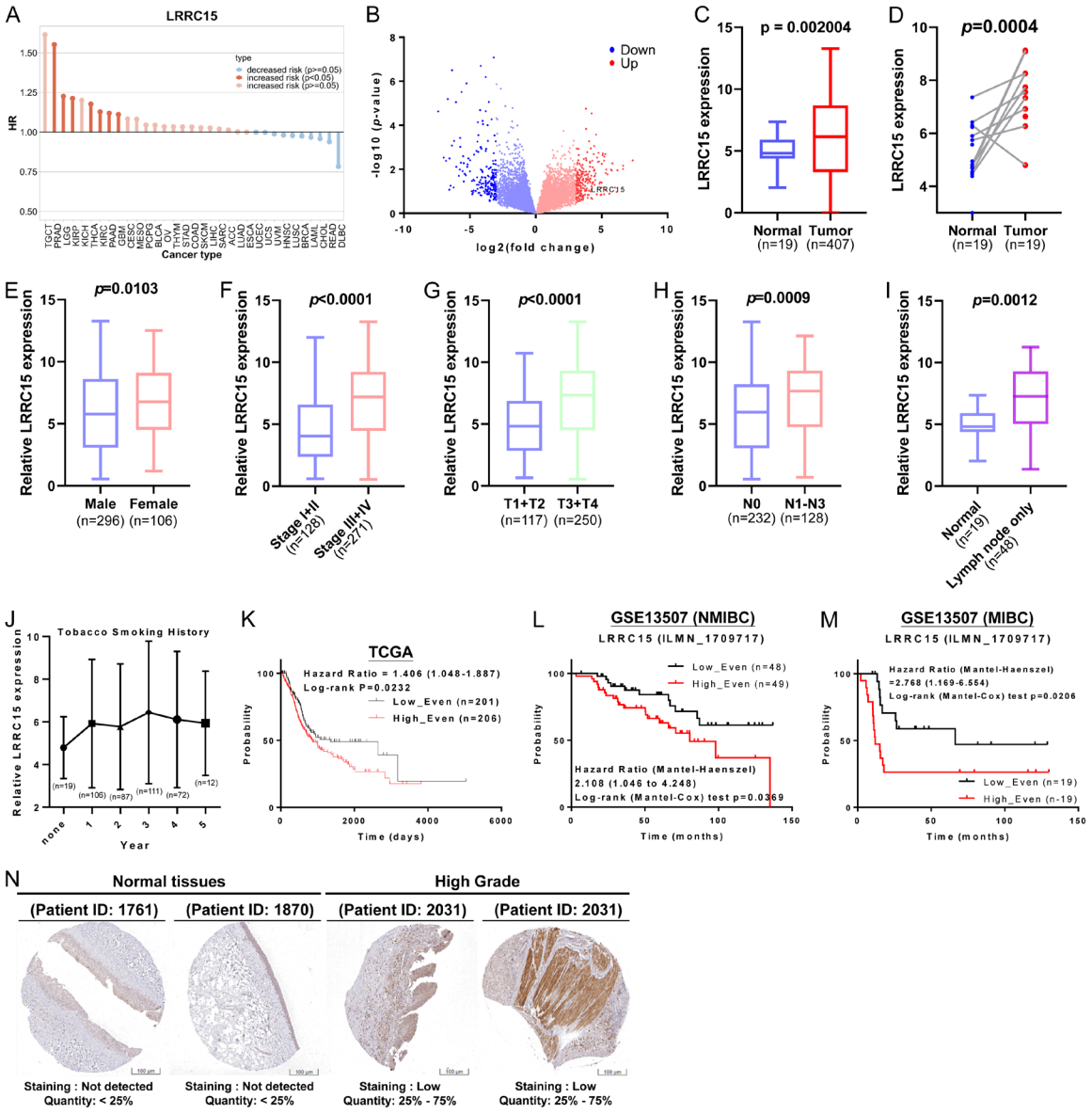

Figure 1. Urothelial carcinoma malignancy is associated with increased LRRC15 expression. A. Hazard ratio analysis delineates the correlation between LRRC15 distribution levels and risk in various cancer patient cohorts. B. Volcano plot illustrating the differential expression levels of LRRC15 between advanced pathological stage IV and early pathological stage I in urothelial carcinoma. C. Transcriptome profiling of LRRC15 in the TCGA-BLCA dataset. D. Comparison of LRRC15 transcriptome levels between paired adjacent normal tissues and corresponding tumor tissues within the TCGA-BLCA cohort. E. Analysis of LRRC15 expression levels across different genders in the TCGA-BLCA dataset. F. Differential analysis of LRRC15 transcriptome levels across various pathological stages in the TCGA-BLCA dataset. G. Variation in LRRC15 transcriptome levels among different pathological T stages in the TCGA-BLCA dataset. H. Differential LRRC15 transcriptome levels across varying pathological N stages in the TCGA-BLCA dataset. I. Transcriptome profiling of LRRC15 in metastatic sites within the TCGA-BLCA cohort. J. Impact of tobacco smoking history on LRRC15 transcriptome levels over time in the TCGA-BLCA dataset. K. Correlation analysis between LRRC15 transcription levels and overall survival rates in the TCGA-BLCA cohort. L. Association between LRRC15 transcription levels and overall survival rates in the non-muscle invasive bladder cancer cohort (GSE13507). M. Correlation of LRRC15 transcription levels with overall survival rates in the muscle invasive bladder cancer cohort (GSE13507). N. Distribution of LRRC15 protein levels in urothelial tissues and carcinoma patient samples.

hazard ratio values suggested a stronger correlation between LRRC15 and MIBC malignancy (**Figure 1L**, **1M**; Supplementary Tables 4, 5). Additionally, immunohistochemistry of urotheli-

al tissues consistently supported transcriptome data, showing high LRRC15 levels in high-grade urothelial carcinoma clinical patient tissues compared to normal tissues (not detected) (**Figure 1N**).

To elucidate the functional significance of LRRC15 in the malignant phenotype of bladder cancer, we employed the T24 cell line, originally derived from a patient with grade III muscle-invasive bladder carcinoma (MIBC). Efficient and sustained silencing of LRRC15 was achieved through lentiviral-mediated shRNA delivery, and immunoblot analysis confirmed robust knockdown at the protein level relative to luciferase shRNA controls (Supplementary Figures 1A, 12). Subsequent phenotypic assessments were conducted using these stable LRRC15-deficient clones. Clonogenic assays revealed a marked suppression in colony-forming capacity upon LRRC15 depletion, indicating a critical role in sustaining proliferative potential ($P = 0.0107$; Supplementary Figure 1B). Furthermore, transwell migration assays performed on fibronectin-coated membranes demonstrated a significant impairment in cellular motility following LRRC15 knockdown ($P = 0.0195$; Supplementary Figure 1C). Similarly, Matrigel-based invasion assays showed a notable reduction in invasive capacity upon LRRC15 silencing ($P = 0.0355$; Supplementary Figure 1D). Collectively, these findings implicate LRRC15 as a key regulator of both growth and motility programs in MIBC-derived T24 cells, highlighting its potential contribution to the aggressive behavior of bladder cancer.

Overall, these clinically relevant findings indicate that increased LRRC15 levels are involved in the pathological events that contribute to malignancy features and serve as a prognostic marker for urothelial carcinoma patients.

LRRC15 contributes to the malignancy of urothelial carcinoma by participating in extracellular matrix organization events

Currently, the molecular mechanism mediated by LRRC15 in cancer biology remains unclear, particularly in urothelial carcinoma. Given the structural composition of the urology system, urothelial carcinoma encompasses both Upper Tract Urothelial Carcinoma (UTUC) and lower tract bladder cancer. Exploring the transcriptome profiles of LRRC15 in these two distinct tissue origins can help map similar or divergent molecular regulations. To investigate the potential mechanisms involving LRRC15, a clinical-based molecular simulated model was employed [34-37]. Initially, molecules significantly positively and negatively correlated with LRRC15 in bladder cancer-related TCGA datasets (Cell 2017, Firehose Legacy, Nature 2014, PanCancer Atlas) were identified using a Venn diagram. Approximately 1919 positive and 276 negative molecules to LRRC15 were identified (Supplementary Figure 2A; Supplementary Table 6). Ingenuity Pathway Analysis (IPA) depicted the potential cellular functions involving LRRC15 in bladder cancer, primarily including cell adhesion, cancer biology, and T lymphocyte-related functions (Supplementary Figure 2B). A ranked gene ontology list highlighted canonical signaling pathways significantly involved in LRRC15 regulation, including Immunoregulatory Interactions between a Lymphoid and a non-Lymphoid cell, Molecular Mechanisms of Cancer, Extracellular Matrix Organization, Integrin Cell Surface Interactions, Tumor Microenvironment Pathway, Axonal Guidance Signaling, Regulation of the Epithelial-Mesenchymal Transition by Growth Factors Pathway, FAK Signaling, ILK Signaling, and Bladder Cancer Signaling (Supplementary Figure 2C; Supplementary Table 7). Among these molecules, potential relationships linked to LRRC15 molecular interaction or regulation were predicted (Supplementary Figure 2D). In UTUC, approximately 2808 positive and 899 negative molecules related to LRRC15 were retrieved from the Cornell/Baylor/MDACC, Nat Commun 2019 dataset. IPA analysis indicated that cellular functions were mainly associated with cell differentiation and cell growth (Supplementary Figure 3A; Supplementary Table 8). Similar to LRRC15 regulation in bladder cancer, but with different rankings, the canonical pathways in UTUC highlighted Molecular Mechanisms of Cancer, Extracellular Matrix Organization, and Axonal Guidance Signaling as primary pathways for tumor progression (Supplementary Figure 3B; Supplementary Table 9). The molecular interaction and regulation map also indicated that LRRC15 participates in UTUC progression through similar or other molecules (Supplementary Figure 3C; Supplementary Table 11). Integrating data from bladder cancer (Supplementary Figure 2) and UTUC (Supplementary Figure 3), approximately

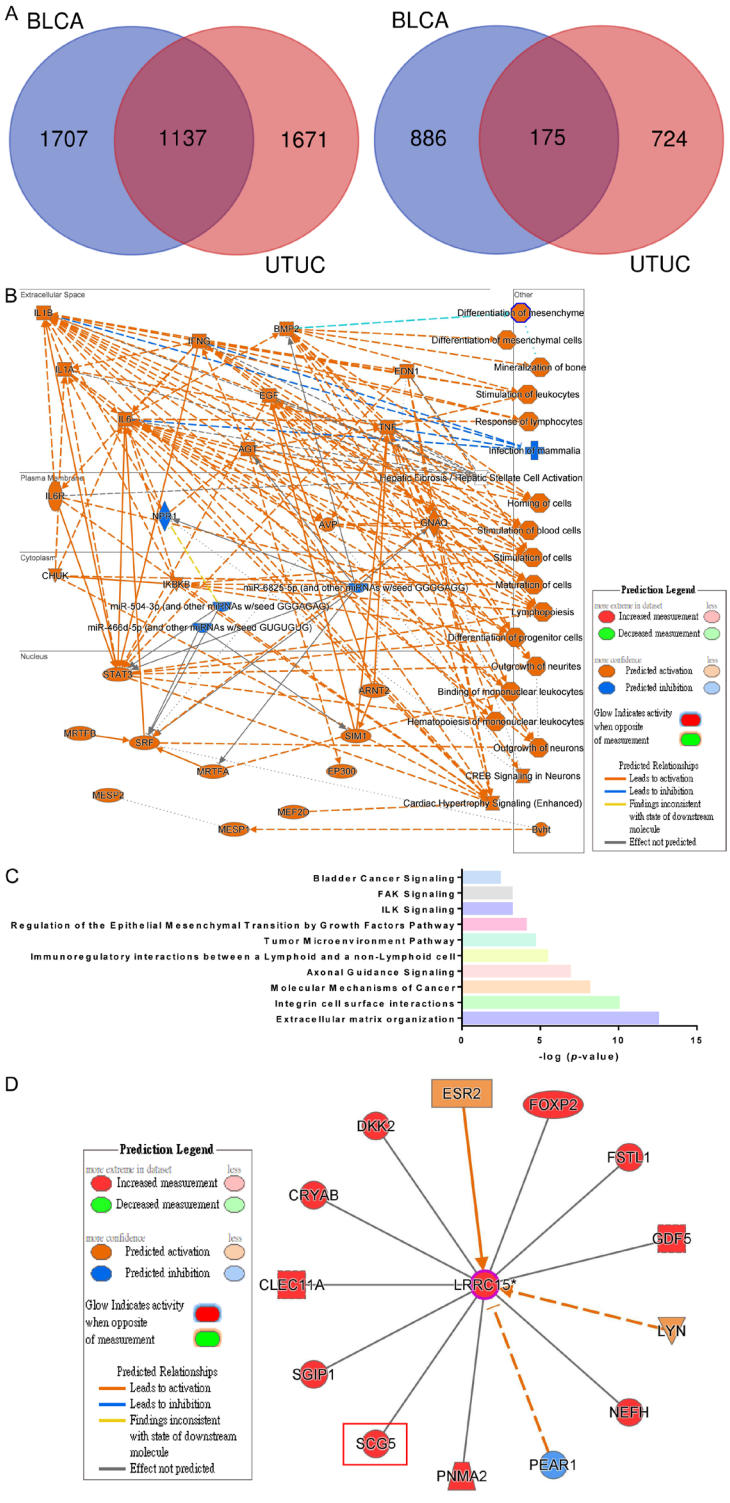

Figure 2. Malignant traits in urothelial carcinoma are regulated by LRRC15 through its participation in extracellular matrix organization. A. Venn diagram analysis identifies molecules that are positively and negatively associated with LRRC15 in bladder cancer and upper tract urothelial carcinoma. B. Graphical summary profile illustrating the key cellular functions of LRRC15 in urothelial carcinoma. C. Gene ontology analysis of LRRC15, detailing its primary co-regulated canonical pathways in urothelial carcinoma. D. Molecular interaction map of LRRC15 highlighting its influence on various molecules in urothelial carcinoma.

1167 positive and 8 negative molecules were found to be co-regulated by LRRC15 in urothelial carcinoma, as analyzed by a Venn diagram (**Figure 2A**). These molecules primarily contribute to cellular functions such as cell differentiation, cell growth, and stimulation of cell-related functions (**Figure 2B**). The ranked canonical pathways showed that Extracellular Matrix Organization, Integrin Cell Surface Interactions, and Molecular Mechanisms of Cancer are significantly regulated by LRRC15 in both bladder cancer and UTUC (**Figure 2C**), mapping the key molecules involved in LRRC15 interaction and regulation (**Figure 2D**). These results suggest that LRRC15 promotes malignancy in urothelial carcinoma through extracellular matrix organization-related signaling, impacting both bladder cancer and UTUC progression.

SCG5 and LRRC15 interaction correlates with specific pathological features in patients with urothelial carcinoma

Based on the results from the clinical-based molecular simulation model, SCG5 emerged as a key molecule due to its role as a chaperone protein that supports the membrane functions of LRRC15 [38]. This consistent link between SCG5 and LRRC15 interaction or regulation in urothelial carcinoma was observed (**Figure 2D**, Supplementary Figures 1D, 2C). A pan-cancer analysis revealed that SCG5 is significantly upregulated in multiple cancers, including urothelial carcinoma (**Figure 3A**). The interactome profile [39] indicated that LRRC15 interacts with SCG5 and shares common interactors (**Figure 3B**; Supplementary Table 12). Transcriptome profiles from TCGA-BLCA showed a significant positive correlation between LRRC15 and

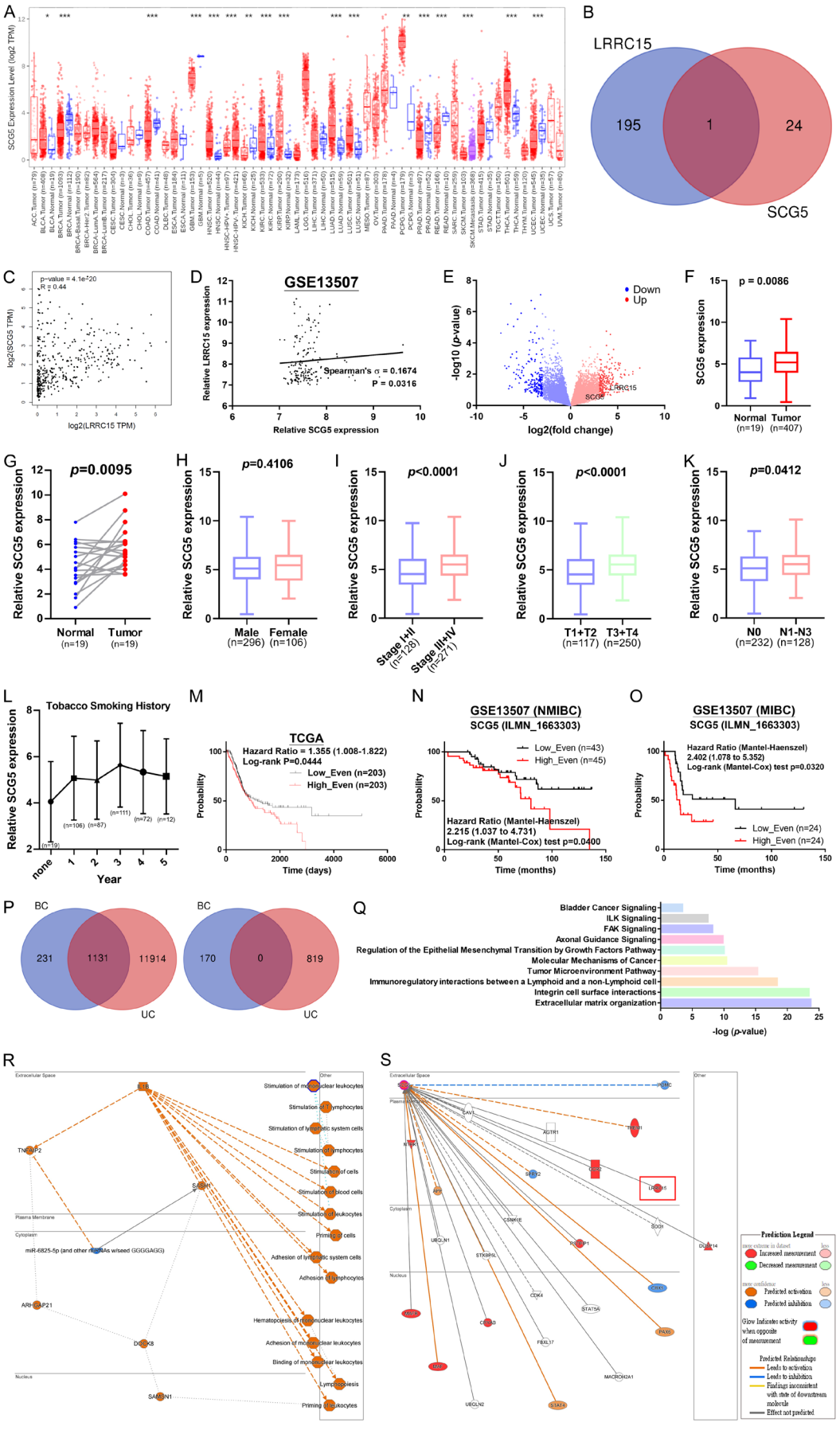
A
SCG5 Expression Level (log2 TPM)
B
LRRC15
195
1
24
SCG5
C
p-value = 4.1e-20
R = 0.44
log2(SCG5 TPM)
log2(LRRC15 TPM)
D
GSE13507
Relative LRRC15 expression
Relative SCG5 expression
Spearman's σ = 0.1674
P = 0.0316
E
Down
Up
-log10 (p-value)
log2(fold change)
LRRC15
SCG5
F
p = 0.0086
SCG5 expression
Normal (n=19)
Tumor (n=407)
G
p=0.0095
Relative SCG5 expression
Normal (n=19)
Tumor (n=19)
H
p=0.4106
Relative SCG5 expression
Male (n=296)
Female (n=106)
I
p<0.0001
Relative SCG5 expression
Stage I+II (n=128)
Stage III+IV (n=271)
J
p<0.0001
Relative SCG5 expression
T1+T2 (n=117)
T3+T4 (n=250)
K
p=0.0412
Relative SCG5 expression
N0 (n=232)
N1-N3 (n=128)
L
Tobacco Smoking History
Relative SCG5 expression
Year
none
M
TCGA
Hazard Ratio = 1.355 (1.008-1.822)
Log-rank P=0.0444
Low_Even (n=203)
High_Even (n=203)
Probability
Time (days)
N
GSE13507 (NMIBC)
SCG5 (ILMN_1663303)
Low_Even (n=43)
High_Even (n=45)
Hazard Ratio (Mantel-Haenszel)
2.215 (1.037 to 4.731)
Log-rank (Mantel-Cox) test p=0.0400
Probability
Time (months)
O
GSE13507 (MIBC)
SCG5 (ILMN_1663303)
Hazard Ratio (Mantel-Haenszel)
2.402 (1.078 to 5.352)
Log-rank (Mantel-Cox) test p=0.0320
Low_Even (n=24)
High_Even (n=24)
Probability
Time (months)
P
BC
231
1131
11914
UC
BC
170
0
819
UC
Q
Bladder Cancer Signaling
ILK Signaling
FAK Signaling
Axonal Guidance Signaling
Regulation of the Epithelial Mesenchymal Transition by Growth Factors Pathway
Molecular Mechanisms of Cancer
Tumor Microenvironment Pathway
Immunoregulatory interactions between a Lymphoid and a non-Lymphoid cell
Integrin cell surface interactions
Extracellular matrix organization
-log (p-value)
R
Extracellular Space
Plasma Membrane
Cytoplasm
Nucleus
Other
Stimulation of monocytes
Stimulation of lymphocytes
Stimulation of lymphatic system cells
Stimulation of lymphocytes
Stimulation of cells
Stimulation of blood cells
Stimulation of leukocytes
Priming of cells
Adhesion of lymphatic system cells
Adhesion of lymphocytes
Hematopoiesis of mononuclear leukocytes
Adhesion of mononuclear leukocytes
Binding of mononuclear leukocytes
Lymphocytolysis
Priming of leukocytes
miR-6825-5p (and other miRNAs w/seed GGGGAGG)
S
Extracellular Space
Plasma Membrane
Cytoplasm
Nucleus
Other
Prediction Legend
Increased measurement
Decreased measurement
Predicted activation
Predicted inhibition
Predicted Relationships
Leads to activation
Leads to inhibition
Findings inconsistent with state of downstream molecule
Effect not predicted

Figure 3. The interaction between SCG5 and LRRC15 is a notable feature in the pathological profiles of urothelial carcinoma patients. A. Distribution of SCG5 levels between normal adjacent and tumor tissues across different cancer types. B. Venn diagram identifying proteins that interact with both LRRC15 and SCG5 based on proteomics profiles. C. Correlation analysis of LRRC15 and SCG5 expression levels in TCGA-BLCA profiles. D. Correlation analysis of LRRC15 and SCG5 expression levels in the bladder cancer cohort (GSE13507). E. Volcano plot depicting SCG5 expression levels in advanced pathological stage IV versus early pathological stage I of urothelial carcinoma. F. Transcriptome profiles of SCG5 in TCGA-BLCA. G. Comparison of SCG5 transcriptome levels between adjacent normal tissues and corresponding tumor tissues in TCGA-BLCA. H. SCG5 expression levels stratified by gender in TCGA-BLCA. I. Differences in SCG5 transcriptome levels across various pathological stages in TCGA-BLCA. J. Variations in SCG5 transcriptome levels across different pathological T stages in TCGA-BLCA. K. Differences in SCG5 transcriptome levels across various pathological N stages in TCGA-BLCA. L. Changes in SCG5 transcriptome levels associated with tobacco smoking history over time in TCGA-BLCA. M. Correlation between SCG5 transcript levels and overall survival rate in TCGA-BLCA. N. Correlation between SCG5 transcript levels and overall survival rate in non-muscle invasive bladder cancer cohort (GSE13507). O. Correlation between SCG5 transcript levels and overall survival rate in muscle invasive bladder cancer cohort (GSE13507). P. Venn diagram identifying molecules positively and negatively associated with SCG5 in bladder cancer and UTUC. Q. Graphical summary profile outlining the primary cellular functions of SCG5 in urothelial carcinoma. R. Gene ontology analysis listing the key canonical pathways co-regulated by SCG5 in urothelial carcinoma. S. Molecular interaction map of SCG5 illustrating its impact on various molecules in urothelial carcinoma.

SCG5 levels (Spearman's correlation = 0.44, P = 4.1E-20). In bladder cancer cohorts, a significant positive correlation between LRRC15 and SCG5 was also observed in NMIBC (Spearman's correlation = 0.1996, P = 0.0443) (Supplementary Figure 4A) and MIBC (Spearman's correlation = 0.1674, P = 0.0316) (Supplementary Figure 4B). Combined analysis of NMIBC and MIBC further confirmed this positive correlation (Spearman's correlation = 0.1674, P = 0.0316) (**Figure 3D**; Supplementary Table 13). Consistent with LRRC15 (**Figure 1B**), SCG5 was found to be upregulated in pathological stage IV tumor tissues compared to stage I in TCGA-BLCA transcriptome profiles (**Figure 3E**). High SCG5 levels were significantly increased in BLCA tissues compared to adjacent normal tissues (P = 0.0086) (**Figure 3F**; Supplementary Table 14). Specifically, comparing identical patients, an increased level of SCG5 in tumor tissues was noted (**Figure 3G**). SCG5 levels did not show significant gender differences among patients (**Figure 3H**). Notably, SCG5 transcriptome levels significantly increased in advanced pathological stages, T and N stages (P < 0.05) (**Figure 3I-K**). Similar to LRRC15, patients with a history of tobacco exposure also showed increased levels of SCG5 (**Figure 3L**). Further linking SCG5 expression profiles to overall survival prognosis revealed that higher SCG5 levels correlated with lower overall survival in TCGA-BLCA patients (P = 0.0444 [HR = 1.335 (1.0008-1.822)]) (**Figure 3M**; Supplementary Table 3). In the bladder-related cohort (GSE13507), high SCG5 levels were associated with worse overall survival rates in NMIBC (P = 0.004 [HR = 2.215 (1.037-4.731)]) (**Figure 3N**; Supplementary Table 4) and MIBC (P = 0.032 [HR = 2.402 (1.078-5.352)]) (**Figure 3O**). To simulate the potential molecular mechanisms of SCG5 in urothelial carcinoma, Venn diagram (Supplementary Figure 5A; Supplementary Table 15) and IPA (Supplementary Figure 5B) analyses were conducted using bladder cancer datasets (Cell 2017, Firehose Legacy, Nature 2014, PanCancer Atlas). SCG5's major cellular functions included cell adhesion and stimulation, primarily via regulation of extracellular matrix organization and integrin cell surface interactions signaling (Supplementary Figure 5C; Supplementary Table 16). Importantly, molecular interaction and regulation analysis confirmed the relationship between SCG5 and LRRC15 (Supplementary Figure 5D). In UTUC, SCG5 primarily influenced cell growth and response to cytotoxicity-related functions (Supplementary Figure 6A; Supplementary Table 17), potentially via ILK signaling and the Th1 pathway (Supplementary Figure 6B; Supplementary Table 18). The molecular interaction and regulation results consistently indicated the relationship between SCG5 and LRRC15 (Supplementary Figure 6C). Combining the positive and negative molecules of SCG5 in both bladder cancer and UTUC (**Figure 3P**; Supplementary Table 19) yielded results consistent with LRRC15, highlighting extracellular matrix organization (**Figure 3Q**; Supplementary Table 20) as the primary canonical pathway influenced by SCG5. As revealed by IPA, the mimic graphical summary derived from SCG5-associated signaling pre-

dicts its involvement in cellular regulatory networks, highlighting potential functional roles and compartmental distribution. Notably, the interaction with LRRC15, delineated within a red-outlined region, suggests a putative molecular axis of relevance (**Figure 3R**, **3S**).

To experimentally validate the biological relevance of SCG5 in bladder cancer progression, we utilized the T24 cell line - a representative MIBC model characterized by aggressive traits. Stable silencing of SCG5 was achieved via lentiviral shRNA transduction, and the efficacy of knockdown was verified through immunoblot analysis (Supplementary Figures 7A, 12). Functionally, suppression of SCG5 resulted in a statistically significant reduction in clonogenic potential, indicative of impaired proliferative capacity (P = 0.0028; Supplementary Figure 7B). Further, transwell-based motility assays demonstrated that SCG5 depletion led to a measurable decline in both cell migration across fibronectin substrates (P = 0.0472; Supplementary Figure 7C) and invasion through Matrigel matrices (P = 0.0044; Supplementary Figure 7D). These findings collectively suggest that SCG5 facilitates tumor-promoting behaviors by augmenting both growth and motility in MIBC-derived cells, thereby implicating it as a potential contributor to bladder cancer aggressiveness. These findings collectively demonstrate that SCG5 is a crucial molecule in LRRC15-mediated urothelial carcinoma malignancy features.

The pathological connection between LRRC15 and SCG5 in patients with urothelial carcinoma

To further validate the relationship between LRRC15 and SCG5 at the molecular level and its reflection in pathological profiles, a series of correlation analyses were conducted. Results demonstrated a significant positive correlation between LRRC15 and SCG5 levels in pathological stages of TCGA-BLCA (Spearman's correlation = 0.4025, P < 0.0001) (**Figure 4A**; Supplementary Table 21). Similar significant correlations were observed in pathological T (Spearman's correlation = 0.4131, P < 0.0001) (**Figure 4B**) and pathological N (Spearman's correlation = 0.4387, P < 0.0001) (**Figure 4C**). Furthermore, analysis using the Cancer Cell Line Encyclopedia (CCLE) datasets indicated that the correlation between LRRC15 and SCG5 observed in pathological profiles was also reflected in BLCA-related cell lines, including absolute profile (Spearman's correlation = 0.6040, P = 0.0029) (**Figure 4D**; Supplementary Table 22) and expression public 23Q4 profile (Spearman's correlation = 0.6846, P < 0.0001) (**Figure 4E**). Combining the prognostic values of LRRC15 (**Figure 1K**) and SCG5 (**Figure 3M**) showed that BLCA patients with higher levels of both LRRC15 and SCG5 had a significantly lower overall survival rate (P = 0.0186) (**Figure 4F**). Additionally, high levels of LRRC15 (P = 0.0478 [HR = 2.888 (1.010-8.254)]) (**Figure 4G**) and SCG5 (P = 0.0351 [HR = 3.091 (1.082-8.830)]) (**Figure 4H**) were significantly associated with worse disease-free interval (DFI) rates. Patients with high levels of both LRRC15 and SCG5 exhibited the worst DFI values (P = 0.029) (**Figure 4I**). Similar findings were observed in the pathological records for progression-free interval (PFI), where high levels of LRRC15 (P = 0.0461 [HR = 1.358 (1.005-1.833)]) (**Figure 4J**) and SCG5 (P = 0.0456 [HR = 1.358 (1.006-1.834)]) (**Figure 4K**) correlated with lower DFI survival rates. Patients with high levels of both LRRC15 and SCG5 had significantly worse DFI values (P = 0.0444) compared to those with low levels of LRRC15 and SCG5 (**Figure 4L**). These results suggest that the molecular regulatory relationship between LRRC15 and SCG5 is reflected in BLCA-related cell lines and patient pathological events.

Prognostic value of effectors within the LRRC15/SCG5 axis in urothelial carcinoma

Following the confirmation of the LRRC15/SCG5 axis as prognostic markers for urothelial carcinoma, the subsequent investigation focused on whether their co-regulated molecules are also involved in tumor malignancy features for prognostic purposes. Molecular analysis of the potential downstream effectors regulated by LRRC15 and SCG5 in urothelial carcinoma (**Figures 2**, **3**) was conducted. Venn diagram analysis further identified downstream effectors co-regulated by both LRRC15 and SCG5 in bladder cancer (**Figure 5A**; Supplementary Table 23), UTUC (**Figure 5B**), and both regions (**Figure 5C**). Ranked gene ontology results from IPA analysis highlighted canonical pathways predominantly affected by both LRRC15 and SCG5, notably extracellular matrix organization

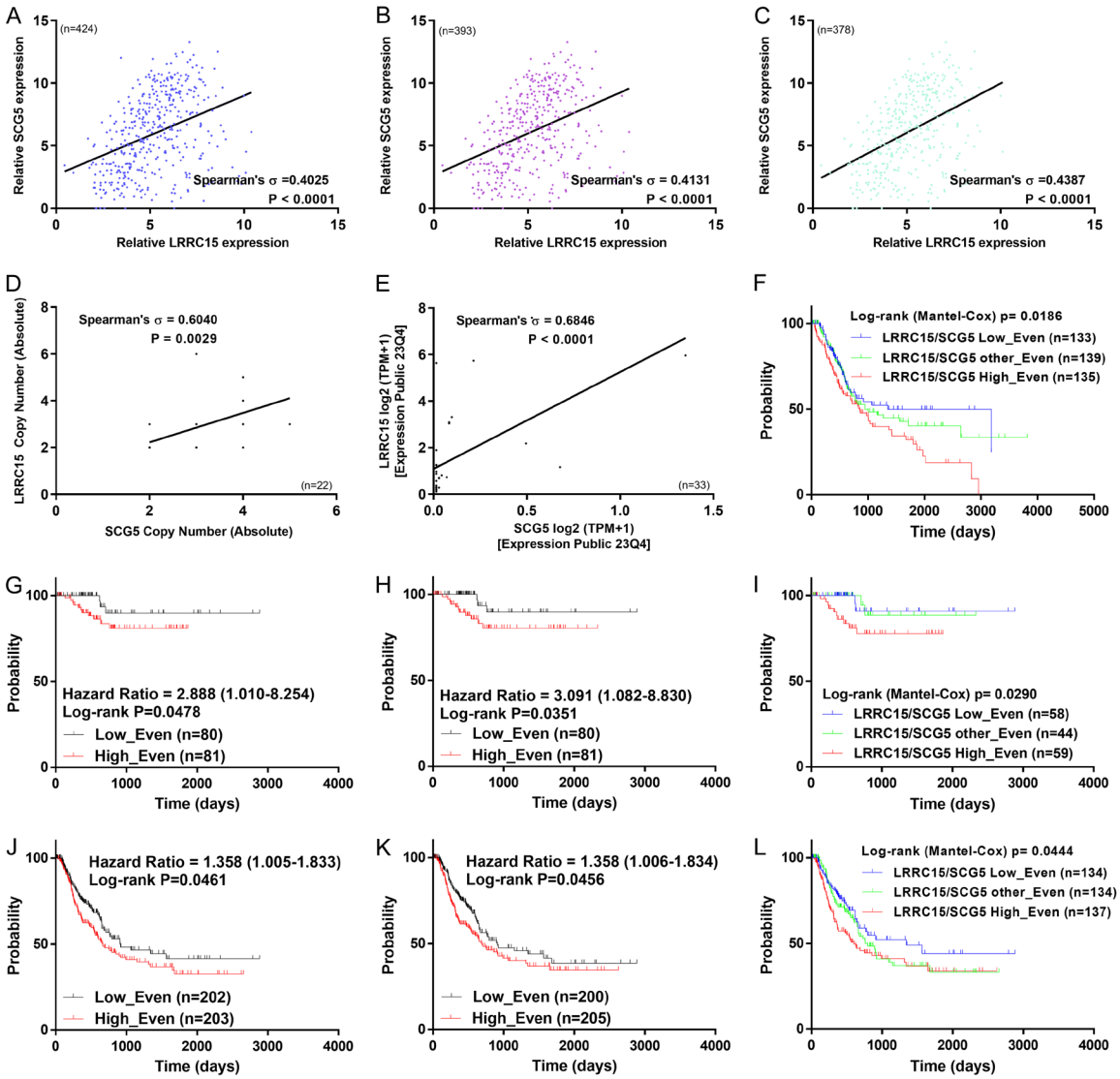

Figure 4. Correlation of LRRC15 and SCG5 in the pathology of urothelial carcinoma patients. A. Correlation between LRRC15 and SCG5 transcriptome levels across different pathological stages in TCGA-BLCA. B. Correlation between LRRC15 and SCG5 transcriptome levels across different pathological T stages in TCGA-BLCA. C. Correlation between LRRC15 and SCG5 transcriptome levels across different pathological N stages in TCGA-BLCA. D. Correlation between LRRC15 and SCG5 transcriptome levels in the Absolute dataset of CCLE-BLCA cell lines. E. Correlation between LRRC15 and SCG5 transcriptome levels in the Expression public 23Q24 dataset of CCLE-BLCA cell lines. F. Prognostic analysis of overall survival in TCGA-BLCA using combined LRRC15 and SCG5 levels. G. Prognostic significance of LRRC15 transcript levels with respect to disease-free interval in TCGA-BLCA. H. Prognostic significance of SCG5 transcript levels with respect to disease-free interval in TCGA-BLCA. I. Prognostic analysis of disease-free interval in TCGA-BLCA incorporating combined LRRC15 and SCG5 levels. J. Prognostic significance of LRRC15 transcript levels with respect to progression-free interval in TCGA-BLCA. K. Prognostic significance of SCG5 transcript levels with respect to progression-free interval in TCGA-BLCA. L. Prognostic analysis of progression-free interval in TCGA-BLCA using combined LRRC15 and SCG5 levels.

and signaling for cell-cell interaction and cell motility in tumor and tumor microenvironment (**Figure 5D-F**; Supplementary Table 24). Molecules regulated by the LRRC15/SCG5 axis in various urothelial carcinoma sources consistently showed significant positive correlation with LRRC15 or SCG5 (Spearman's correlation = 0.3, $P < 0.05$) (**Figure 5G-I**). Importantly, downstream effectors mediated by the LRRC15/SCG5 axis further demonstrated their

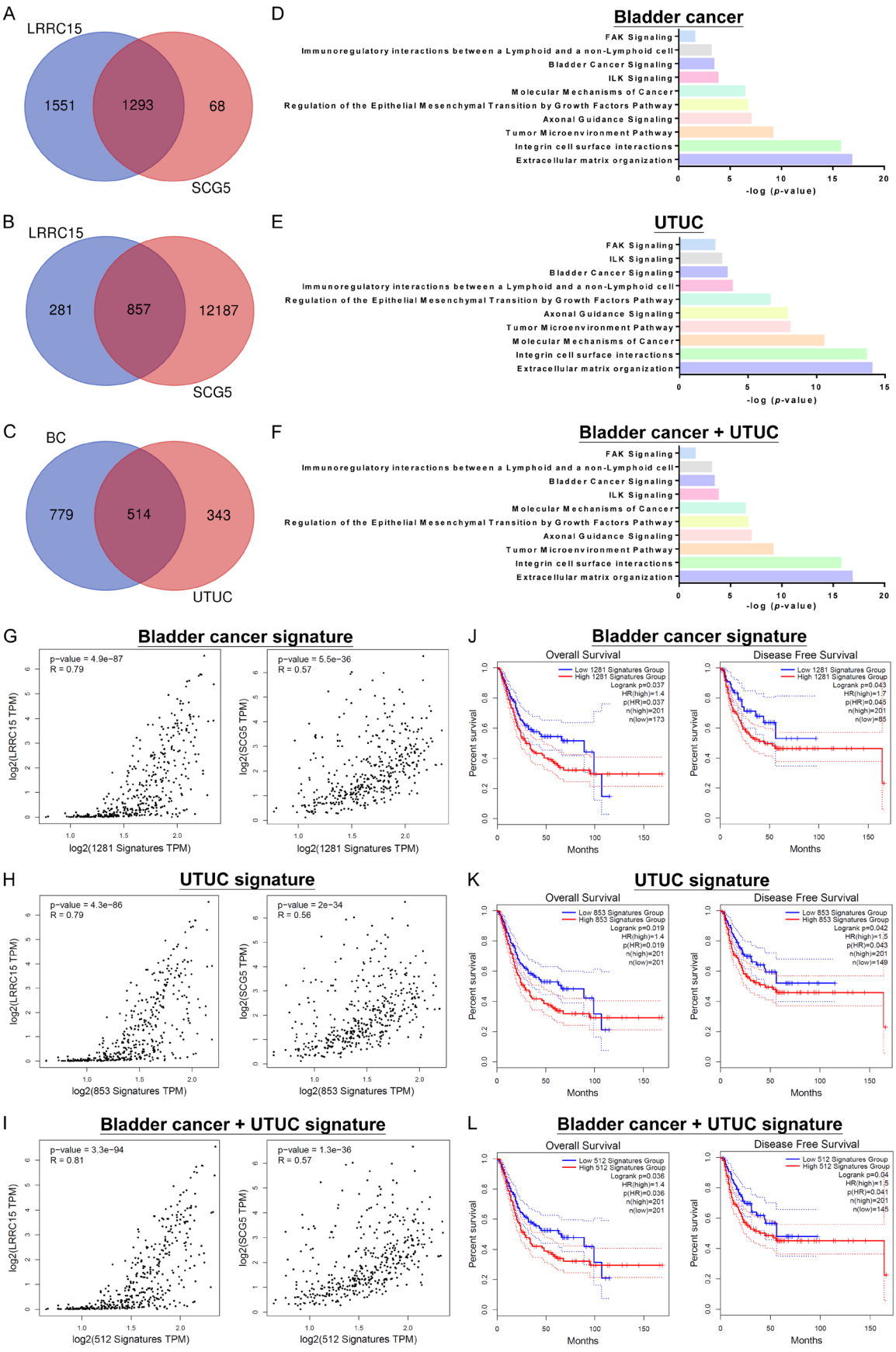
A
LRRC15
1551
1293
68
SCG5
B
LRRC15
281
857
12187
SCG5
C
BC
779
514
343
UTUC
D
Bladder cancer
FAK Signaling
Immunoregulatory interactions between a Lymphoid and a non-Lymphoid cell
Bladder Cancer Signaling
ILK Signaling
Molecular Mechanisms of Cancer
Regulation of the Epithelial Mesenchymal Transition by Growth Factors Pathway
Axonal Guidance Signaling
Tumor Microenvironment Pathway
Integrin cell surface interactions
Extracellular matrix organization
-log (p-value)
E
UTUC
FAK Signaling
ILK Signaling
Bladder Cancer Signaling
Immunoregulatory interactions between a Lymphoid and a non-Lymphoid cell
Regulation of the Epithelial Mesenchymal Transition by Growth Factors Pathway
Axonal Guidance Signaling
Tumor Microenvironment Pathway
Molecular Mechanisms of Cancer
Integrin cell surface interactions
Extracellular matrix organization
-log (p-value)
F
Bladder cancer + UTUC
FAK Signaling
Immunoregulatory interactions between a Lymphoid and a non-Lymphoid cell
Bladder Cancer Signaling
ILK Signaling
Molecular Mechanisms of Cancer
Regulation of the Epithelial Mesenchymal Transition by Growth Factors Pathway
Axonal Guidance Signaling
Tumor Microenvironment Pathway
Integrin cell surface interactions
Extracellular matrix organization
-log (p-value)
G
Bladder cancer signature
p-value = 4.9e-87
R = 0.79
log2(LRRC15 TPM)
log2(1281 Signatures TPM)
p-value = 5.5e-36
R = 0.57
log2(SCG5 TPM)
log2(1281 Signatures TPM)
H
UTUC signature
p-value = 4.3e-86
R = 0.79
log2(LRRC15 TPM)
log2(853 Signatures TPM)
p-value = 2e-34
R = 0.56
log2(SCG5 TPM)
log2(853 Signatures TPM)
I
Bladder cancer + UTUC signature
p-value = 3.3e-94
R = 0.81
log2(LRRC15 TPM)
log2(512 Signatures TPM)
p-value = 1.3e-36
R = 0.57
log2(SCG5 TPM)
log2(512 Signatures TPM)
J
Bladder cancer signature
Overall Survival
Low 1281 Signatures Group
High 1281 Signatures Group
Logrank p=0.037
HR(high)=1.4
p(HR)=0.037
n(high)=201
n(low)=173
Percent survival
Months
Disease Free Survival
Low 1281 Signatures Group
High 1281 Signatures Group
Logrank p=0.043
HR(high)=1.7
p(HR)=0.045
n(high)=201
n(low)=85
Percent survival
Months
K
UTUC signature
Overall Survival
Low 853 Signatures Group
High 853 Signatures Group
Logrank p=0.019
HR(high)=1.4
p(HR)=0.019
n(high)=201
n(low)=201
Percent survival
Months
Disease Free Survival
Low 853 Signatures Group
High 853 Signatures Group
Logrank p=0.042
HR(high)=1.5
p(HR)=0.043
n(high)=201
n(low)=149
Percent survival
Months
L
Bladder cancer + UTUC signature
Overall Survival
Low 512 Signatures Group
High 512 Signatures Group
Logrank p=0.036
HR(high)=1.4
p(HR)=0.036
n(high)=201
n(low)=201
Percent survival
Months
Disease Free Survival
Low 512 Signatures Group
High 512 Signatures Group
Logrank p=0.04
HR(high)=1.5
p(HR)=0.041
n(high)=201
n(low)=145
Percent survival
Months

Figure 5. The impact of LRRC15/SCG5 axis effectors on prognostic markers in urothelial carcinoma. A. Venn diagram illustrating co-regulated molecules between LRRC15 and SCG5 in TCGA-BLCA datasets. B. Venn diagram depicting co-regulated molecules between LRRC15 and SCG5 in the UTUC dataset. C. Venn diagram showing co-regulated molecules between LRRC15 and SCG5 across TCGA-BLCA and UTUC datasets. D. Canonical pathways involving co-regulated molecules of the LRRC15/SCG5 axis in bladder cancer. E. Canonical pathways associated with co-regulated molecules of the LRRC15/SCG5 axis in UTUC. F. Canonical pathways shared by co-regulated molecules of the LRRC15/SCG5 axis in both bladder cancer and UTUC. G. Correlation between co-regulated molecules and the LRRC15/SCG5 axis as a bladder cancer signature. H. Correlation between co-regulated molecules and the LRRC15/SCG5 axis as a UTUC signature. I. Correlation between co-regulated molecules and the LRRC15/SCG5 axis as a signature for both bladder cancer and UTUC. J. Prognostic value of the LRRC15/SCG5-mediated bladder cancer signature for overall survival and disease-free survival. K. Prognostic value of the LRRC15/SCG5-mediated UTUC signature for overall survival and disease-free survival. L. Prognostic significance of the LRRC15/SCG5-mediated signature in bladder cancer and UTUC for overall survival and disease-free survival.

potential as signatures for overall survival and disease-free survival prognostic purposes ($P < 0.05$, $HR > 1$) (**Figure 5J-L**).

To further dissect the regulatory interplay between LRRC15 and SCG5 and its relevance to clinical prognosis in bladder cancer, we systematically examined their interdependence in vitro using individual knockdown clones (Supplementary Figures 1, 7). Surprisingly, quantitative PCR analysis revealed that silencing either LRRC15 or SCG5 led to a significant downregulation of the reciprocal gene at the transcript level, suggesting a bidirectional regulatory circuit (Supplementary Figures 8A, 11, 12). Consistently, immunoblotting confirmed that depletion of LRRC15 resulted in a concomitant reduction of SCG5 protein abundance (Supplementary Figure 8B), reinforcing the existence of a functional LRRC15-SCG5 axis that may contribute to malignancy beyond correlative transcriptomic profiles observed in patient cohorts. This molecular linkage prompted further exploration of its therapeutic vulnerability. As a proof-of-concept, we employed Samrotamab - a humanized IgG1-κ chimeric monoclonal antibody targeting LRRC15. Treatment of bladder cancer cells with Samrotamab markedly reduced tumor cell viability compared to the IgG isotype control (Supplementary Figure 8D vs. Supplementary Figure 8C). Moreover, Samrotamab exposure led to a paradoxical compensatory upregulation of LRRC15 transcripts ($P = 0.0031$), while simultaneously suppressing SCG5 mRNA expression ($P = 0.0011$; Supplementary Figure 8E), providing mechanistic support that LRRC15 inhibition disrupts the downstream axis driving malignant phenotypes. Functional assays validated the therapeutic implications of LRRC15 blockade. Samrotamab-treated cells exhibited significantly diminished clonogenic growth capacity ($P = 0.0317$; Supplementary Figure 8F), indicating effective suppression of tumor cell propagation. Furthermore, transwell-based assays revealed substantial reductions in migratory ($P = 0.0389$; Supplementary Figure 8G) and invasive ($P = 0.0106$; Supplementary Figure 8H) capabilities, highlighting the efficacy of targeting the LRRC15-SCG5 signaling module in curtailing bladder cancer aggressiveness.

Together, these comprehensive analysis results support that the LRRC15/SCG5 axis indeed participates in the progression of urothelial carcinoma by promoting malignancy features. The LRRC15/SCG5 axis and its effectors serve as valuable prognostic markers and signatures for urothelial carcinoma.

Discussion

The heterogeneity of urothelial carcinoma partly stems from variations in tumorigenesis across different patients within the urinary system. Based on pathological stages, bladder cancer is further classified into non-muscle invasive (NMIBC) and muscle invasive (MIBC) subtypes. Although transurethral resection of bladder tumors (TURBT) can remove tumors and preserve normal organ function, combined with additional therapeutic strategies for preventive intervention, nearly 20% of patients experience recurrence [10]. With the advancement of artificial intelligence, deep learning approaches are increasingly employed to identify potential biomarkers for cancer prognosis and targeted therapy. Identifying markers involved in the progression of urothelial carcinoma from various origins will enhance the precision of patient prognosis and facilitate the development of tailored clinical treatments.

In this study, an in-silico model identified LRRC15 as being involved in various tumor pro-

gressions and associated with high-risk survival rates (**Figure 1A**), a finding that aligns with previous reports in glioblastoma, ovarian cancer, and breast cancer [16-18]. This study represents the first comprehensive investigation into the potential role of LRRC15 in urothelial carcinoma. Analysis of clinical transcriptome profiles from TCGA-BLCA datasets confirmed that LRRC15 expression is significantly elevated in advanced pathological stages (**Figure 1B**). Comparative analysis revealed a notable increase in LRRC15 levels in tumor tissues compared to normal adjacent tissues, with significant differences observed not only between individuals (**Figure 1C**) but also within identical patients (**Figure 1D**). Variations in LRRC15 transcript levels were found to distinguish between different pathological features, including pathological stages (**Figure 1F**), T stages (**Figure 1G**), and N stages (**Figure 1H**). Immunohistochemistry further supported these findings, showing elevated LRRC15 levels in high-grade urothelial carcinoma tissues (**Figure 1N**). Clinical data suggest that changes in LRRC15 expression may be influenced by hormonal and tobacco exposure (**Figure 1E** and **1J**). Moreover, the association between LRRC15 and advanced pathological features, along with prognosis events and transcriptome profiles from TCGA-BLCA, highlights that high LRRC15 levels correlate with poor overall survival (**Figure 1K**). Notably, LRRC15 is linked to worse overall survival predictions in both NMIBC (**Figure 1L**) and MIBC (**Figure 1M**; Supplementary Table 5), with significance and hazard ratio values indicating a stronger correlation with reduced survival rates in MIBC. Consequently, LRRC15 emerges as a promising target for prognosis and therapeutic intervention in urothelial carcinoma. In this study, we employed clinical transcriptome profiles from bladder cancer and UTUC to develop a molecular simulation model [34-37] aimed at mapping the LRRC15-mediated gene ontology across different tissue origins of urothelial carcinoma. The analysis revealed that in bladder cancer, LRRC15 is predicted to be involved in cellular adhesion, cancer-related mechanisms, and microenvironmental cellular functions (Supplementary Figure 2B). Conversely, in UTUC, LRRC15 is predominantly associated with tumor growth-related functions (Supplementary Figure 3A; Supplementary Table 10). Notably, LRRC15's impact on cellular differentiation and growth is evident in both bladder cancer and UTUC (**Figure 2A**). Gene ontology analyses of LRRC15-mediated cellular functions highlight that canonical pathways include extracellular matrix organization (**Figure 2C**), although the ranking of these pathways differs slightly between bladder cancer (Supplementary Figure 2C) and UTUC (Supplementary Figure 3B). LRRC15 has been previously reported to promote tumor metastasis features in ovarian and breast cancer [19, 20]. Moreover, it has been shown to regulate integrin-related signaling to enhance ovarian cancer cell motility [24]. Consistent with these findings, our ranked canonical pathways list confirms the involvement of integrin cell surface interactions, ILK, and FAK signaling in LRRC15 regulation in both bladder cancer (Supplementary Figure 2C) and UTUC (Supplementary Figure 3B), reinforcing the designation of LRRC15 as an adhesion protein antigen [23]. Beyond tumor cells, LRRC15 is also distributed in fibroblasts, including corneal and periodontal ligament-associated fibroblasts [27, 28], suggesting its potential as a biomarker for tumor microenvironment [40]. Previous reports have identified LRRC15 expression in various cancer-associated fibroblasts, implicating it in immunosuppressive activities and extracellular matrix remodeling [29-32]. Studies have shown that activated or mesenchymal fibroblasts can transactivate LRRC15 expression through TGFβ [29, 30]. Additionally, in breast cancer, artificial manipulation of LRRC15 in cancer-associated fibroblasts has been found to affect Wnt/β-catenin signaling, influencing breast cancer cell motility features [32]. Although transcriptomic analysis of TCGA-BLCA datasets revealed a statistically significant positive correlation among LRRC15, SCG5, and TGFβ expression in patient-derived tumors (Supplementary Figure 9), this coordinated upregulation was not recapitulated in our stem-like T24 cell model. Specifically, the LRRC15-SCG5 axis did not display a notable elevation in the $CD133^{high}/CD44^{high}$ tumor sphere-enriched subpopulation (Supplementary Figure 10), suggesting that this molecular circuit may not be directly involved in sustaining cancer stemness phenotypes or may be uncoupled under sphere-forming conditions.

Our molecular simulation model underscores that LRRC15's roles extend beyond tumor-specific functions, including significant involvement in tumor microenvironment pathways

and immunoregulatory interactions between lymphoid and non-lymphoid cells (**Figure 2C**, Supplementary Figures 2C, 3B). These findings collectively suggest that LRRC15 plays a multifaceted role in urothelial carcinoma, impacting both tumor progression and the surrounding microenvironment.

The integration of literature and molecular simulation model results suggests that LRRC15-mediated pathways involving extracellular matrix organization and tumor microenvironment in urothelial carcinoma may implicate interactions with cancer-associated fibroblasts. Research on LRRC15 distribution within membrane regions indicates that its protein-protein interaction partners could be leveraged for designing strategies to enhance drug delivery and efficacy [41]. This study identifies SCG5 as a critical factor in the molecular interaction and regulation of LRRC15 in both bladder cancer (Supplementary Figure 2D) and UTUC (Supplementary Figure 3C). The interactome profile supports the interaction between LRRC15 and SCG5 [39]. Transcriptome analysis from TCGA-BLCA and the bladder cancer-related cohort (GSE13507) shows that the expression of both LRRC15 and SCG5 is elevated in bladder cancer patients (**Figure 3C**, **3D**). SCG5, like LRRC15, is significantly increased in tumor tissues (**Figure 3F**, **3G**) and is upregulated in advanced pathological stages (**Figure 3I**), pathological T (**Figure 3J**), and pathological N (**Figure 3K**). Additionally, SCG5 levels increase in response to tobacco exposure over time (**Figure 3L**). Unlike LRRC15, which exhibits higher levels in females compared to males (**Figure 1E**), SCG5 levels are not significantly influenced by gender (**Figure 3H**). In urothelial carcinoma patients, elevated SCG5 levels are associated with worse prognosis outcomes, including in non-muscle invasive bladder cancer (NMIBC) (**Figure 3N**) and muscle invasive bladder cancer (MIBC) (**Figure 3O**; Supplementary Table 5). This is consistent with findings in renal cell carcinoma and tongue cancer, where SCG5 is linked to poor overall survival rates [42-44]. Conversely, in pancreatic cancer, SCG5 is downregulated in malignant tumors, suggesting a potential tumor-suppressive role [21]. These findings underscore the potential of LRRC15 and SCG5 as biomarkers and therapeutic targets in urothelial carcinoma, providing insights into their roles in tumor progression and response to treatment.

In urothelial carcinoma, a significant correlation between the expression levels of LRRC15 and SCG5 is observed across patient cohorts, including various pathological stages, pathological T, and pathological N classifications (**Figure 4A-C**). Notably, this correlation is not limited to patient samples but is also evident in transcriptome profiles from commercially available urothelial carcinoma cell lines (**Figure 4D**, **4E**). The correlation between LRRC15 and SCG5 expression levels is further reflected in overall survival, disease-free interval, and progression-free interval metrics (**Figure 4F-L**; Supplementary Table 3), consistently identifying patients with high LRRC15 and SCG5 levels as having a higher risk and poorer treatment response. The role of LRRC15 as a prognostic marker has been previously associated with chemoresistance in osteosarcoma [25]. Additionally, upregulation of LRRC15 has been noted during the progression to androgen-independent prostate cancer [26]. Interestingly, membrane-bound LRRC15 has been shown to rearrange cell surface receptors, potentially affecting the efficiency of adenovirus-based therapeutic agents [15]. Furthermore, Bacillus Calmette-Guérin (BCG) therapy, used as adjuvant treatment for non-muscle invasive bladder cancer (NMIBC), interacts with extracellular matrix components such as integrins and fibronectin [45]. Given the previously noted association between LRRC15 and integrin, it is plausible that LRRC15 expression may influence patient tolerance to BCG therapy [23, 24]. Currently, targeted therapies using LRRC15-specific antibody-drug conjugates (ADCs) are in clinical trials [29]. Combining LRRC15-targeted ADCs, such as ABBV-085, with BCG treatment may enhance therapeutic efficacy and potentially reduce patient resistance. This approach warrants further investigation as a strategy to improve outcomes in NMIBC. Collectively, the evidence from this study, including the pathological correlation between LRRC15 and SCG5 in urothelial carcinoma and the molecular simulations, demonstrates that the LRRC15/SCG5 axis not only serves as an effective prognostic marker but also that their co-regulated downstream effectors provide valuable signatures for predicting outcomes in bladder and UTUC. Targeting the LRRC15/SCG5 axis could significantly enhance diagnostic and therapeutic strategies for urothelial carcinoma, offering potential advancements in clinical management and treatment efficacy.

Materials and methods

Transcriptome profiles of LRRC15 and SCG5 in urothelial carcinoma

Transcriptome profiles for LRRC15 and SCG5 in urothelial carcinoma were sourced from multiple databases, including TCGA-BLCA (https://portal.gdc.cancer.gov/projects/TCGA-BLCA), GEPIA2 (http://gepia2.cancer-pku.cn/#index), and Timer 2.0 (http://timer.comp-genomics.org/timer/). These profiles were used to evaluate the distribution of gene expression in relation to tumor characteristics, pathological stages, survival outcomes, gender, and tobacco history. Correlations between LRRC15 and SCG5 expression levels and overall survival rates in NMIBC and MIBC were analyzed using transcriptome data from GSE13507 (https://www.ncbi.nlm.nih.gov/geo/query/acc.cgi?acc=GSE13507).

Distribution of LRRC15 protein in clinical tissues of urothelial carcinoma

Immunohistochemical staining of LRRC15 protein was conducted on tissue samples from normal urinary bladder and urothelial carcinoma patients. The staining results were visualized using images and associated staining scores provided by the Human Protein Atlas (https://www.proteinatlas.org/). These data were systematically organized and presented in the figures of this study to illustrate the differential expression patterns of LRRC15 across different tissue types and patient cohorts.

Clinical-based molecular simulation model of the LRRC15/SCG5 axis

Molecular interaction models were constructed based on clinical data and previously established methodologies [34-37]. Spearman correlation scores of +0.3 and -0.3 were utilized to assess the relationships among LRRC15, SCG5, and their co-regulated downstream effectors across datasets, including TCGA (PanCancer Atlas, Nature 2014; Firehose Legacy; Cell 2017) and the UTUC dataset (Cornell/Baylor/MDACC, Nat Commun 2019). Significant molecular interactions were identified through Venn diagram analysis and further analyzed using Ingenuity Pathway Analysis to elucidate potential cellular functions, gene ontology, and molecular interactions relevant to urothelial carcinoma.

Correlation of LRRC15 and SCG5 in urothelial carcinoma

The correlation between LRRC15 and SCG5 in urothelial carcinoma was assessed using data from the Cancer Cell Line Encyclopedia (CCLE) database (https://sites.broadinstitute.org/ccle/). Both the absolute profile and the expression public 23Q4 profile datasets were downloaded and analyzed. Statistical software was employed to compute and analyze the correlation between these two proteins.

Establishment of long-term gene silencing models targeting LRRC15 and SCG5 in human T24 bladder cancer cells

T24 cells, representing high-grade bladder carcinoma, were procured from FIRDI (Taiwan) and subsequently maintained under standard culture protocols. To support optimal cell viability, cultures were incubated in McCoy's 5A medium supplemented with 10% fetal bovine serum and antibiotics (1% pen-strep) under physiological conditions. Mycoplasma surveillance was routinely carried out using polymerase chain reaction techniques to validate the sterility of cell cultures. Gene-specific shRNA constructs targeting LRRC15 and SCG5 were procured from the National RNAi Core Facility (Academia Sinica, Taiwan) to facilitate stable knockdown cell line generation. To generate lentivirus harboring the desired shRNA, HEK293T cells were co-transfected with pLKO.1-puro, pCMVΔR8.91, and pMD.G plasmids using Lipofectamine 3000, following standardized protocols. Culture media enriched with lentiviral particles were retrieved 48 and 72 hours after transfection, filtered to remove cellular debris using a 0.45-μm membrane, and employed to infect T24 cells alongside 8 μg/mL polybrene. A 7-day selection protocol using puromycin at a concentration of 2 μg/mL was employed to enrich for cells harboring stable shRNA-mediated gene silencing. The suppression levels of LRRC15 and SCG5 transcripts and proteins were quantitatively evaluated using real-time PCR and Western blot analyses, respectively. Total RNA extraction was performed using TRIzol reagent, followed by reverse transcription into cDNA utilizing the TOOLSQuant II Fast RT Kit (BIOTOOLS, KRT-BA06-2) according to the manufacturer's guidelines. Real-time PCR assays employed SYBR Green chemistry on a QuantStudio 1 instrument, and gene expres-

sion was quantified relative to 18S rRNA using the 2^-ΔΔCt approach. Total protein was extracted by lysing cells in radioimmunoprecipitation assay buffer enriched with inhibitors targeting both serine/threonine phosphatases and broad-spectrum proteases. Equalized protein inputs, following concentration assessment, were fractionated via SDS-polyacrylamide gel electrophoresis and immobilized on PVDF membranes using electrotransfer. To minimize background signal, membranes were incubated in a 5% bovine serum albumin solution and subsequently exposed overnight at 4°C to primary antibodies specific for LRRC15 (Cell signaling, 50546), SCG5 (Proteintech, 10761-1-AP), and β-actin (GeneTex, GT5512). Following incubation with horseradish peroxidase-conjugated secondary antibodies, chemiluminescent signals were visualized using the ChemiDoc imaging platform in accordance with the ECL detection protocol.

Dissecting the oncogenic potential of LRRC15 and SCG5 in bladder carcinoma progression

To delineate the contributions of LRRC15, SCG5, and Samrotamab to bladder tumor pathobiology, we conducted a panel of in vitro assays focused on cellular proliferation and invasiveness. Samrotamab at 20 μg/mL (MCE, catalog HY-P99899) was administered for a 24-hour period, with Human IgG1 kappa isotype control (HY-P99001) included as a reference to assess subsequent biological responses. A clonogenic assay was performed by seeding 500 LRRC15- and SCG5-silenced T24 bladder carcinoma cells per well in standard 6-well culture dishes to evaluate long-term proliferative capacity. Routine maintenance of the cells was carried out in McCoy's 5A medium fortified with 10% FBS and antibiotic-antimycotic agents, with complete medium replacement performed every 72 hours. At the end of a two-week culture period, colonies were stabilized via 4% paraformaldehyde treatment and stained with 0.1% crystal violet to enable downstream visualization. Quantification of colony formation was performed by manual inspection, wherein each colony was operationally defined as a cell cluster composed of no fewer than 50 individual cells. Migration and invasion capacities were evaluated using Boyden chambers equipped with transwell filters featuring 8-μm pores, with migration assays employing fibronectin-coated membranes and invasion assays utilizing Matrigel-coated inserts. Cells of the T24 line were subjected to serum starvation for one day prior to plating at a density of 100,000 cells per insert in McCoy's 5A medium devoid of fetal bovine serum. Cells were seeded into the upper compartment of the transwell, while the lower chamber was filled with medium enriched with 10% fetal bovine serum to serve as a chemotactic stimulus. To simulate the extracellular matrix barrier, the upper chamber was coated with a Matrigel layer at a concentration of 1 mg/mL prior to cell seeding for invasion assays. After allowing cells to migrate or invade for 24 hours, those that failed to traverse the membrane were delicately wiped away from the upper chamber with a cotton tip. After translocation to the membrane's lower side, cells were preserved with 4% paraformaldehyde, stained with a crystal violet solution, and assessed by counting in three arbitrarily selected areas per well using bright-field microscopy. Data were represented as the mean cell count per microscopic field for both migrated and invaded populations.

Statistical significance of clinicopathological correlations of the LRRC15/SCG5 axis and kaplan-meier plotter analysis in urothelial carcinoma

Clinical and pathological correlations, as well as prognostic analyses, including Kaplan-Meier plots, were computed using Microsoft Office 2019 and SPSS version 19. The significance of associations between transcriptome profiles of LRRC15 and SCG5 in urothelial carcinoma patients was evaluated using unpaired Student's t-tests. Statistical significance was denoted as follows: *$P < 0.05$, **$P < 0.01$, and ***$P < 0.001$.

Acknowledgements

We gratefully acknowledge Taipei Medical University and Shuang Ho Hospital for their provision of the hardware and software resources required for the successful execution of the analytical work in this study. This study was supported by grants from Taipei Medical University-Shuang Ho Hospital, Taiwan (grant number: 114TMU-SHH-32 and 114FRP-23), awarded to C. H. L. and C. C. W., and by the National Science and Technology Council of Taiwan (grant 113-2314-B-038-033), awarded to K. Y. T. and C. C. W.

Disclosure of conflict of interest

None.

Abbreviations

NMIBC, Non-muscle invasive bladder cancer; MIBC, Muscle invasive bladder cancer; LRRC15, Leucine-rich repeat containing 15; LRRC, Leucine-rich repeat-containing; LRR, Leucine-rich repeat; TCGA, The Cancer Genome Atlas Program; UTUC, Upper Tract Urothelial Carcinoma; IPA, Ingenuity Pathway Analysis; CCLE, Cancer Cell Line Encyclopedia; DFI, Disease-free interval; PFI, Progression-free interval; TURBT, Transurethral resection of bladder tumors; BCG, Bacillus Calmette-Guérin; ADCs, Antibody-drug conjugates.

Address correspondence to: Drs. Chia-Chang Wu and Chien Hsiu Li, Department of Urology, Taipei Medical University-Shuang Ho Hospital, Ministry of Health and Welfare, New Taipei, Taiwan. Tel: +886-2-2249-0088; E-mail: 08253@s.tmu.edu.tw (CCW); 23510@s.tmu.edu.tw (CHL)

References

[1] Siegel RL, Giaquinto AN and Jemal A. Cancer statistics, 2024. CA Cancer J Clin 2024; 74: 12-49.

[2] Saginala K, Barsouk A, Aluru JS, Rawla P, Padala SA and Barsouk A. Epidemiology of bladder cancer. Med Sci (Basel) 2020; 8: 15.

[3] Fujii Y, Sato Y, Suzuki H, Kakiuchi N, Yoshizato T, Lenis AT, Maekawa S, Yokoyama A, Takeuchi Y, Inoue Y, Ochi Y, Shiozawa Y, Aoki K, Yoshida K, Kataoka K, Nakagawa MM, Nannya Y, Makishima H, Miyakawa J, Kawai T, Morikawa T, Shiraishi Y, Chiba K, Tanaka H, Nagae G, Sanada M, Sugihara E, Sato TA, Nakagawa T, Fukayama M, Ushiku T, Aburatani H, Miyano S, Coleman JA, Homma Y, Solit DB, Kume H and Ogawa S. Molecular classification and diagnostics of upper urinary tract urothelial carcinoma. Cancer Cell 2021; 39: 793-809, e798.

[4] Rothman N, Garcia-Closas M, Chatterjee N, Malats N, Wu X, Figueroa JD, Real FX, Van Den Berg D, Matullo G, Baris D, Thun M, Kiemeney LA, Vineis P, De Vivo I, Albanes D, Purdue MP, Rafnar T, Hildebrandt MA, Kiltie AE, Cussenot O, Golka K, Kumar R, Taylor JA, Mayordomo JI, Jacobs KB, Kogevinas M, Hutchinson A, Wang Z, Fu YP, Prokunina-Olsson L, Burdett L, Yeager M, Wheeler W, Tardon A, Serra C, Carrato A, Garcia-Closas R, Lloreta J, Johnson A, Schwenn M, Karagas MR, Schned A, Andriole G Jr, Grubb R 3rd, Black A, Jacobs EJ, Diver WR, Gapstur SM, Weinstein SJ, Virtamo J, Cortessis VK, Gago-Dominguez M, Pike MC, Stern MC, Yuan JM, Hunter DJ, McGrath M, Dinney CP, Czerniak B, Chen M, Yang H, Vermeulen SH, Aben KK, Witjes JA, Makkinje RR, Sulem P, Besenbacher S, Stefansson K, Riboli E, Brennan P, Panico S, Navarro C, Allen NE, Bueno-de-Mesquita HB, Trichopoulos D, Caporaso N, Landi MT, Canzian F, Ljungberg B, Tjonneland A, Clavel-Chapelon F, Bishop DT, Teo MT, Knowles MA, Guarrera S, Polidoro S, Ricceri F, Sacerdote C, Allione A, Cancel-Tassin G, Selinski S, Hengstler JG, Dietrich H, Fletcher T, Rudnai P, Gurzau E, Koppova K, Bolick SC, Godfrey A, Xu Z, Sanz-Velez JI, D García-Prats M, Sanchez M, Valdivia G, Porru S, Benhamou S, Hoover RN, Fraumeni JF Jr, Silverman DT and Chanock SJ. A multistage genome-wide association study of bladder cancer identifies multiple susceptibility loci. Nat Genet 2010; 42: 978-984.

[5] Freedman ND, Silverman DT, Hollenbeck AR, Schatzkin A and Abnet CC. Association between smoking and risk of bladder cancer among men and women. JAMA 2011; 306: 737-745.

[6] Brandau S and Bohle A. Bladder cancer. I. Molecular and genetic basis of carcinogenesis. Eur Urol 2001; 39: 491-497.

[7] Abern MR, Dude AM, Tsivian M and Coogan CL. The characteristics of bladder cancer after radiotherapy for prostate cancer. Urol Oncol 2013; 31: 1628-1634.

[8] Kaufman DS, Shipley WU and Feldman AS. Bladder cancer. Lancet 2009; 374: 239-249.

[9] Slovacek H, Zhuo J and Taylor JM. Approaches to non-muscle-invasive bladder cancer. Curr Oncol Rep 2021; 23: 105.

[10] Teoh JY, Kamat AM, Black PC, Grivas P, Shariat SF and Babjuk M. Recurrence mechanisms of non-muscle-invasive bladder cancer - a clinical perspective. Nat Rev Urol 2022; 19: 280-294.

[11] Sylvester RJ, van der Meijden AP, Oosterlinck W, Witjes JA, Bouffioux C, Denis L, Newling DW and Kurth K. Predicting recurrence and progression in individual patients with stage Ta T1 bladder cancer using EORTC risk tables: a combined analysis of 2596 patients from seven EORTC trials. Eur Urol 2006; 49: 466-465.

[12] Carrasco R, Ingelmo-Torres M, Gomez A, Trullas R, Roldan FL, Ajami T, Moreno D, Rodriguez-Carunchio L, Alcaraz A, Izquierdo L and Mengual L. Cell-Free DNA as a prognostic biomarker for monitoring muscle-invasive bladder cancer. Int J Mol Sci 2022; 23: 11732.

[13] Del Pozo Jimenez G, Herranz Amo F, Arranz Arija JA, Rodriguez Fernandez E, Subira Rios D, Lledo Garcia E, Bueno Chomon G, Cancho Gil MJ, Carballido Rodriguez J and Hernandez

Fernandez C. Effect of adjuvant chemotherapy in locally advanced urothelial carcinoma of the bladder treated with cystectomy. Actas Urol Esp (Engl Ed) 2020; 44: 94-102.
[14] Chakraborty J. A comprehensive review of soybean RNL and TIR domain proteins. Plant Mol Biol 2024; 114: 78.
[15] O'Prey J, Wilkinson S and Ryan KM. Tumor antigen LRRC15 impedes adenoviral infection: implications for virus-based cancer therapy. J Virol 2008; 82: 5933-5939.
[16] Tang H, Liu W, Xu Z, Zhao J, Wang W, Yu Z and Wei M. Integrated microenvironment-associated genomic profiles identify LRRC15 mediating recurrent glioblastoma-associated macrophages infiltration. J Cell Mol Med 2021; 25: 5534-5546.
[17] Zhu X, You S, Du X, Song K, Lv T, Zhao H and Yao Q. LRRC superfamily expression in stromal cells predicts the clinical prognosis and platinum resistance of ovarian cancer. BMC Med Genomics 2023; 16: 10.
[18] Mendonca JB, Fernandes PV, Fernandes DC, Rodrigues FR, Waghabi MC and Tilli TM. Unlocking overexpressed membrane proteins to guide breast cancer precision medicine. Cancers (Basel) 2024; 16: 1402.
[19] Mariani A, Wang C, Oberg AL, Riska SM, Torres M, Kumka J, Multinu F, Sagar G, Roy D, Jung DB, Zhang Q, Grassi T, Visscher DW, Patel VP, Jin L, Staub JK, Cliby WA, Weroha SJ, Kalli KR, Hartmann LC, Kaufmann SH, Goode EL and Shridhar V. Genes associated with bowel metastases in ovarian cancer. Gynecol Oncol 2019; 154: 495-504.
[20] Schuetz CS, Bonin M, Clare SE, Nieselt K, Sotlar K, Walter M, Fehm T, Solomayer E, Riess O, Wallwiener D, Kurek R and Neubauer HJ. Progression-specific genes identified by expression profiling of matched ductal carcinomas in situ and invasive breast tumors, combining laser capture microdissection and oligonucleotide microarray analysis. Cancer Res 2006; 66: 5278-5286.
[21] Xu JS, Liao KL, Wang X, He J and Wang XZ. Combining bioinformatics techniques to explore the molecular mechanisms involved in pancreatic cancer metastasis and prognosis. J Cell Mol Med 2020; 24: 14128-14138.
[22] Satoh K, Hata M and Yokota H. A novel member of the leucine-rich repeat superfamily induced in rat astrocytes by beta-amyloid. Biochem Biophys Res Commun 2002; 290: 756-762.
[23] Ray U, Pathoulas CL, Thirusangu P, Purcell JW, Kannan N and Shridhar V. Exploiting LRRC15 as a novel therapeutic target in cancer. Cancer Res 2022; 82: 1675-1681.
[24] Ray U, Jung DB, Jin L, Xiao Y, Dasari S, Sarkar Bhattacharya S, Thirusangu P, Staub JK, Roy D, Roy B, Weroha SJ, Hou X, Purcell JW, Bakkum-Gamez JN, Kaufmann SH, Kannan N, Mitra AK and Shridhar V. Targeting LRRC15 inhibits metastatic dissemination of ovarian cancer. Cancer Res 2022; 82: 1038-1054.
[25] Cui J, Dean D, Wei R, Hornicek FJ, Ulmert D and Duan Z. Expression and clinical implications of leucine-rich repeat containing 15 (LRRC15) in osteosarcoma. J Orthop Res 2020; 38: 2362-2372.
[26] Stanbrough M, Bubley GJ, Ross K, Golub TR, Rubin MA, Penning TM, Febbo PG and Balk SP. Increased expression of genes converting adrenal androgens to testosterone in androgen-independent prostate cancer. Cancer Res 2006; 66: 2815-2825.
[27] Miron-Mendoza M, Poole K, DiCesare S, Nakahara E, Bhatt MP, Hulleman JD and Petroll WM. The role of vimentin in human corneal fibroblast spreading and myofibroblast transformation. Cells 2024; 13: 1094.
[28] Kim HJ, Kim DJ, Kim SM and Jang YJ. Leucine-rich repeat containing 15-mediated cell adhesion is essential for integrin signaling in TGF-beta1-induced PDL fibroblastic differentiation. Stem Cells 2024; 42: 251-265.
[29] Purcell JW, Tanlimco SG, Hickson J, Fox M, Sho M, Durkin L, Uziel T, Powers R, Foster K, McGonigal T, Kumar S, Samayoa J, Zhang D, Palma JP, Mishra S, Hollenbaugh D, Gish K, Morgan-Lappe SE, Hsi ED and Chao DT. LRRC15 is a novel mesenchymal protein and stromal target for antibody-drug conjugates. Cancer Res 2018; 78: 4059-4072.
[30] Krishnamurty AT, Shyer JA, Thai M, Gandham V, Buechler MB, Yang YA, Pradhan RN, Wang AW, Sanchez PL, Qu Y, Breart B, Chalouni C, Dunlap D, Ziai J, Elstrott J, Zacharias N, Mao W, Rowntree RK, Sadowsky J, Lewis GD, Pillow TH, Nabet BY, Banchereau R, Tam L, Caothien R, Bacarro N, Roose-Girma M, Modrusan Z, Mariathasan S, Muller S and Turley SJ. LRRC15(+) myofibroblasts dictate the stromal setpoint to suppress tumour immunity. Nature 2022; 611: 148-154.
[31] Dominguez CX, Muller S, Keerthivasan S, Koeppen H, Hung J, Gierke S, Breart B, Foreman O, Bainbridge TW, Castiglioni A, Senbabaoglu Y, Modrusan Z, Liang Y, Junttila MR, Klijn C, Bourgon R and Turley SJ. Single-cell RNA sequencing reveals stromal evolution into LRRC15(+) myofibroblasts as a determinant of patient response to cancer immunotherapy. Cancer Discov 2020; 10: 232-253.
[32] Yang Y, Wu H, Fan S, Bi Y, Hao M and Shang J. Cancer-associated fibroblast-derived LRRC15 promotes the migration and invasion of triple-negative breast cancer cells via Wnt/beta-catenin signalling pathway regulation. Mol Med Rep 2022; 25: 2.

[33] Jubber I, Ong S, Bukavina L, Black PC, Comperat E, Kamat AM, Kiemeney L, Lawrentschuk N, Lerner SP, Meeks JJ, Moch H, Necchi A, Panebianco V, Sridhar SS, Znaor A, Catto JWF and Cumberbatch MG. Epidemiology of bladder cancer in 2023: a systematic review of risk factors. Eur Urol 2023; 84: 176-190.

[34] Li CH, Chan MH and Chang YC. The role of fructose 1,6-bisphosphate-mediated glycolysis/gluconeogenesis genes in cancer prognosis. Aging (Albany NY) 2022; 14: 3233-3258.

[35] Li CH, Chan MH, Chang YC and Hsiao M. The CHST11 gene is linked to lung cancer and pulmonary fibrosis. J Gene Med 2022; 24: e3451.

[36] Li CH, Fang CY, Chan MH, Lu PJ, Ger LP, Chu JS, Chang YC, Chen CL and Hsiao M. The activation of EP300 by F11R leads to EMT and acts as a prognostic factor in triple-negative breast cancers. J Pathol Clin Res 2023; 9: 165-181.

[37] Li CH, Fang CY, Chan MH, Chen CL, Chang YC and Hsiao M. The cytoplasmic expression of FSTL3 correlates with colorectal cancer progression, metastasis status and prognosis. J Cell Mol Med 2023; 27: 672-686.

[38] Farber CR, Chitwood J, Lee SN, Verdugo RA, Islas-Trejo A, Rincon G, Lindberg I and Medrano JF. Overexpression of Scg5 increases enzymatic activity of PCSK2 and is inversely correlated with body weight in congenic mice. BMC Genet 2008; 9: 34.

[39] Huttlin EL, Bruckner RJ, Navarrete-Perea J, Cannon JR, Baltier K, Gebreab F, Gygi MP, Thornock A, Zarraga G, Tam S, Szpyt J, Gassaway BM, Panov A, Parzen H, Fu S, Golbazi A, Maenpaa E, Stricker K, Guha Thakurta S, Zhang T, Rad R, Pan J, Nusinow DP, Paulo JA, Schweppe DK, Vaites LP, Harper JW and Gygi SP. Dual proteome-scale networks reveal cell-specific remodeling of the human interactome. Cell 2021; 184: 3022-3040, e3028.

[40] Qiao H, Lv R, Pang Y, Yao Z, Zhou X, Zhu W and Zhou W. Weighted gene coexpression network analysis identifies TBC1D10C as a new prognostic biomarker for breast cancer. Anal Cell Pathol (Amst) 2022; 2022: 5259187.

[41] Cao S, Peterson SM, Muller S, Reichelt M, McRoberts Amador C and Martinez-Martin N. A membrane protein display platform for receptor interactome discovery. Proc Natl Acad Sci U S A 2021; 118: e2025451118.

[42] Sakaguchi T, Yoshino H, Sugita S, Miyamoto K, Yonemori M, Osako Y, Meguro-Horike M, Horike SI, Nakagawa M and Enokida H. Bromodomain protein BRD4 inhibitor JQ1 regulates potential prognostic molecules in advanced renal cell carcinoma. Oncotarget 2018; 9: 23003-23017.

[43] Lv X and Yu X. Signatures and prognostic values of related immune targets in tongue cancer. Front Surg 2023; 9: 952389.

[44] Xin Y, Jiang Q, Liu C and Qiu J. Plumbagin has an inhibitory effect on the growth of TSCC PDX model and it enhances the anticancer efficacy of cisplatin. Aging (Albany NY) 2023; 15: 12225-12250.

[45] Redelman-Sidi G, Glickman MS and Bochner BH. The mechanism of action of BCG therapy for bladder cancer–a current perspective. Nat Rev Urol 2014; 11: 153-162.

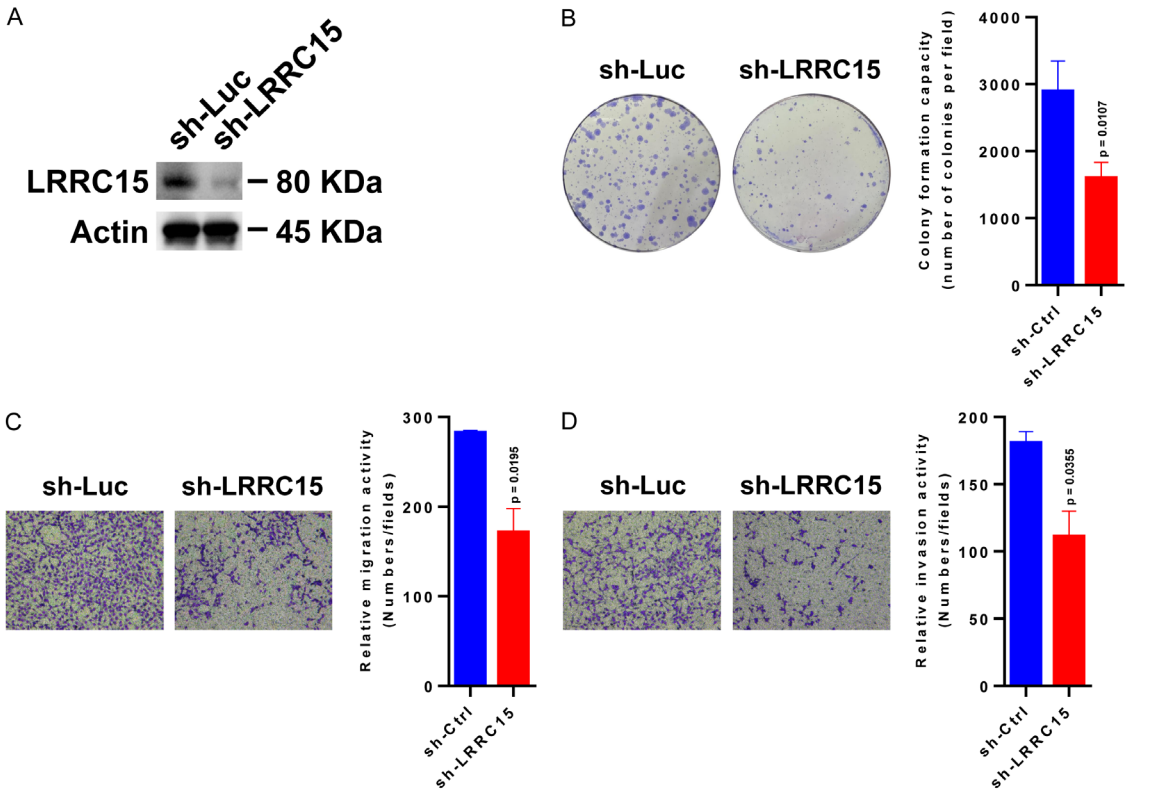

Supplementary Figure 1. LRRC15 loss as a modulator of tumorigenic and invasive traits in bladder cancer. A. The suppression efficiency of LRRC15 achieved via lentiviral-mediated knockdown was validated through immunoblot analysis. B. Silencing LRRC15 markedly impaired the clonogenic capacity of T24 bladder carcinoma cells under adherent conditions. C. Targeted suppression of LRRC15 curtailed the migratory potential of T24 urothelial carcinoma cells under serum gradient stimulation. D. LRRC15 depletion weakened the ability of bladder cancer cells to navigate and invade through artificial extracellular matrix substrates.

A

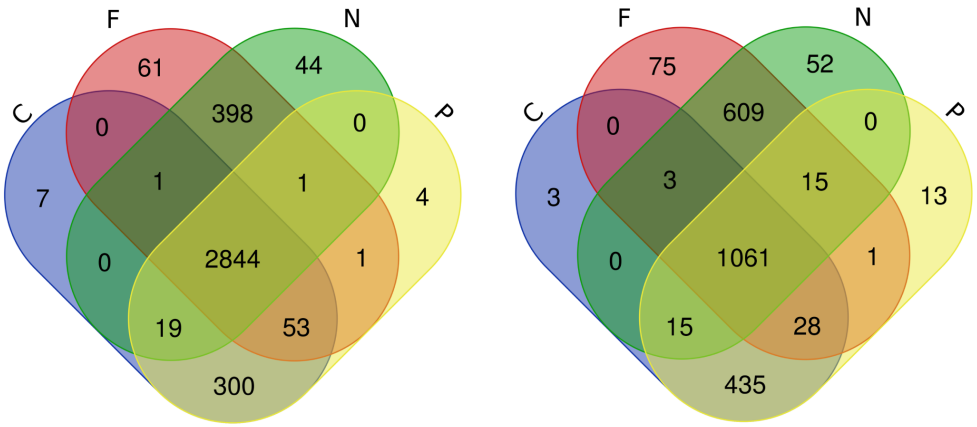
F
N
C
P
61
44
0
398
0
7
1
1
4
0
2844
1
19
53
300
F
N
C
P
75
52
0
609
0
3
3
15
13
0
1061
1
15
28
435

B

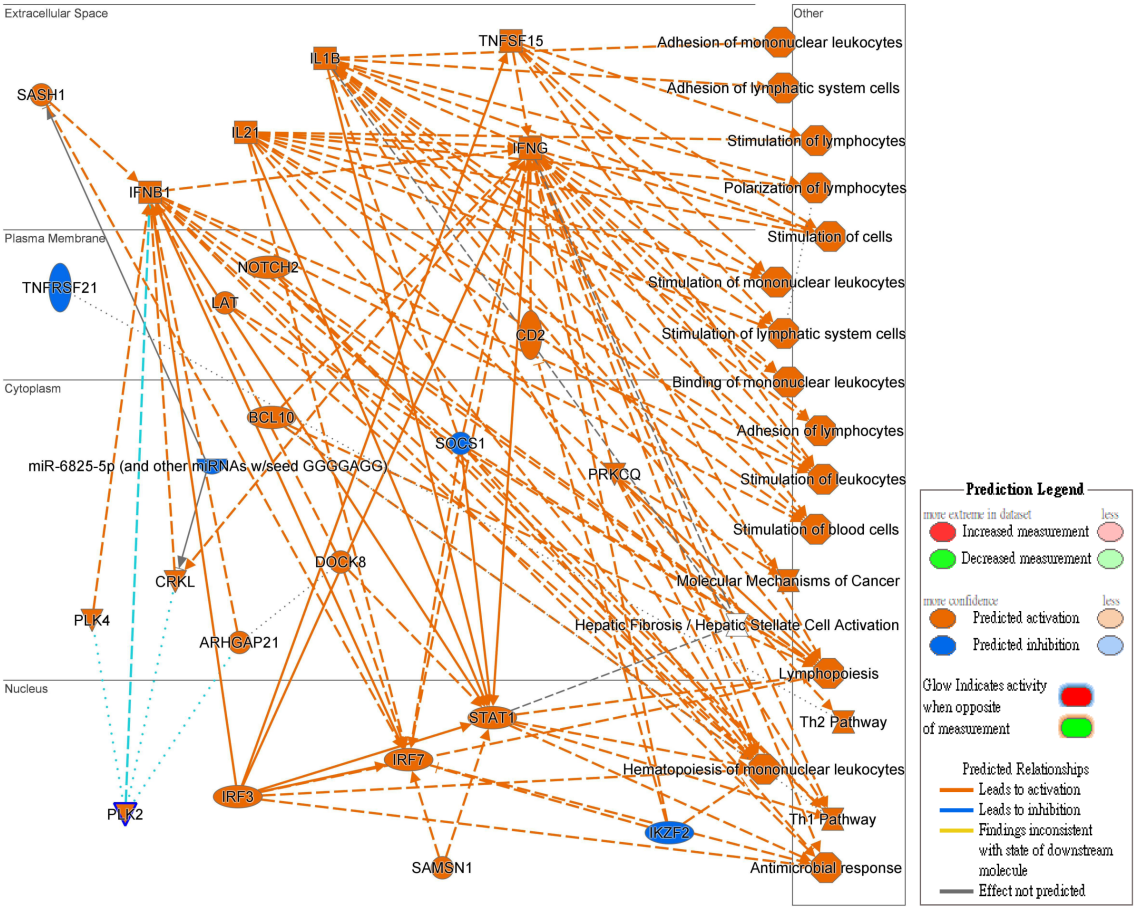
Extracellular Space
Plasma Membrane
Cytoplasm
Nucleus
Other
TNFSF15
IL1B
SASH1
IL21
IFNG
IFNB1
NOTCH2
TNFRSF21
LAT
CD2
BCL10
SOCS1
miR-6825-5p (and other miRNAs w/seed GGGGAGG)
PRKCQ
DOCK8
CRKL
PLK4
ARHGAP21
STAT1
IRF7
IRF3
PLK2
SAMSN1
IKZF2
Adhesion of mononuclear leukocytes
Adhesion of lymphatic system cells
Stimulation of lymphocytes
Polarization of lymphocytes
Stimulation of cells
Stimulation of mononuclear leukocytes
Stimulation of lymphatic system cells
Binding of mononuclear leukocytes
Adhesion of lymphocytes
Stimulation of leukocytes
Stimulation of blood cells
Molecular Mechanisms of Cancer
Hepatic Fibrosis / Hepatic Stellate Cell Activation
Lymphopoiesis
Th2 Pathway
Hematopoiesis of mononuclear leukocytes
Th1 Pathway
Antimicrobial response
Prediction Legend
more extreme in dataset
less
Increased measurement
Decreased measurement
more confidence
less
Predicted activation
Predicted inhibition
Glow Indicates activity when opposite of measurement
Predicted Relationships
Leads to activation
Leads to inhibition
Findings inconsistent with state of downstream molecule
Effect not predicted

C

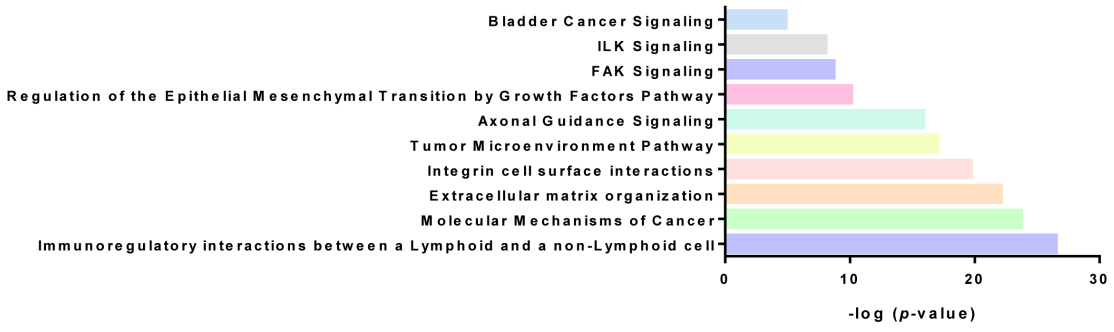
Bladder Cancer Signaling
ILK Signaling
FAK Signaling
Regulation of the Epithelial Mesenchymal Transition by Growth Factors Pathway
Axonal Guidance Signaling
Tumor Microenvironment Pathway
Integrin cell surface interactions
Extracellular matrix organization
Molecular Mechanisms of Cancer
Immunoregulatory interactions between a Lymphoid and a non-Lymphoid cell
0
10
20
30
-log (p-value)

D

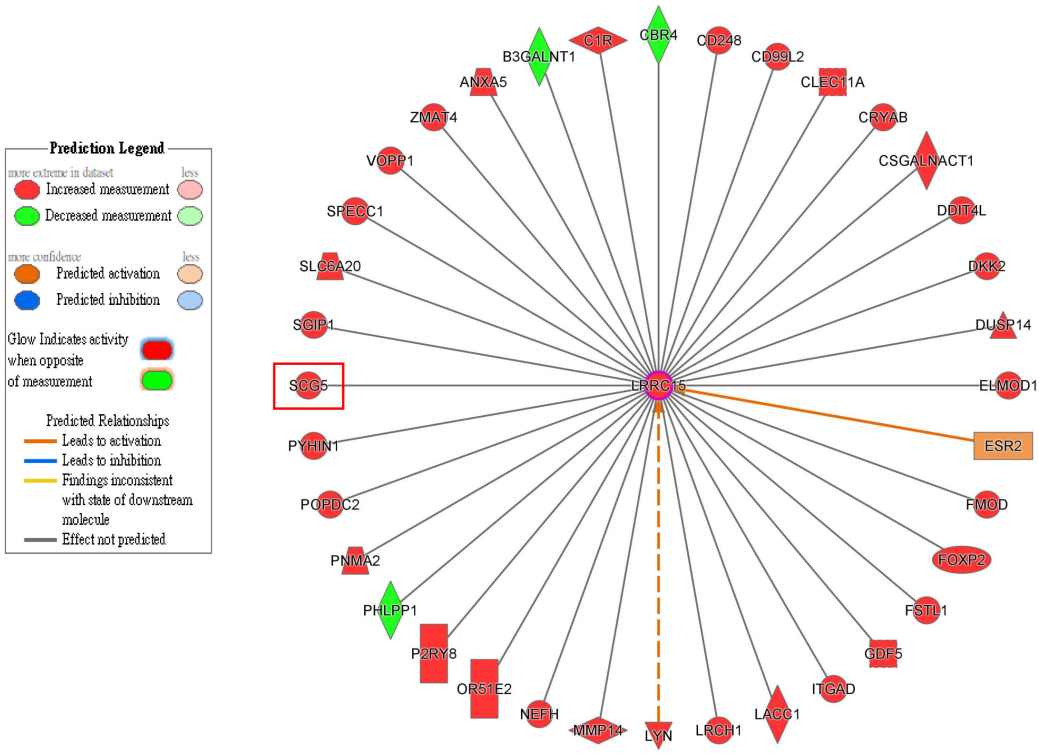

Supplementary Figure 2. Biological functions and molecular regulations of LRRC15 in bladder cancer. A. Venn diagram illustrating the identification of molecules positively and negatively associated with LRRC15 in bladder cancer. B. Graphical summary profile depicting the key cellular functions associated with LRRC15 in bladder cancer. C. Gene Ontology analysis outlining the canonical pathways regulated by LRRC15 in bladder cancer. D. Molecular interaction map of LRRC15, highlighting the impacted molecules in bladder cancer.

A

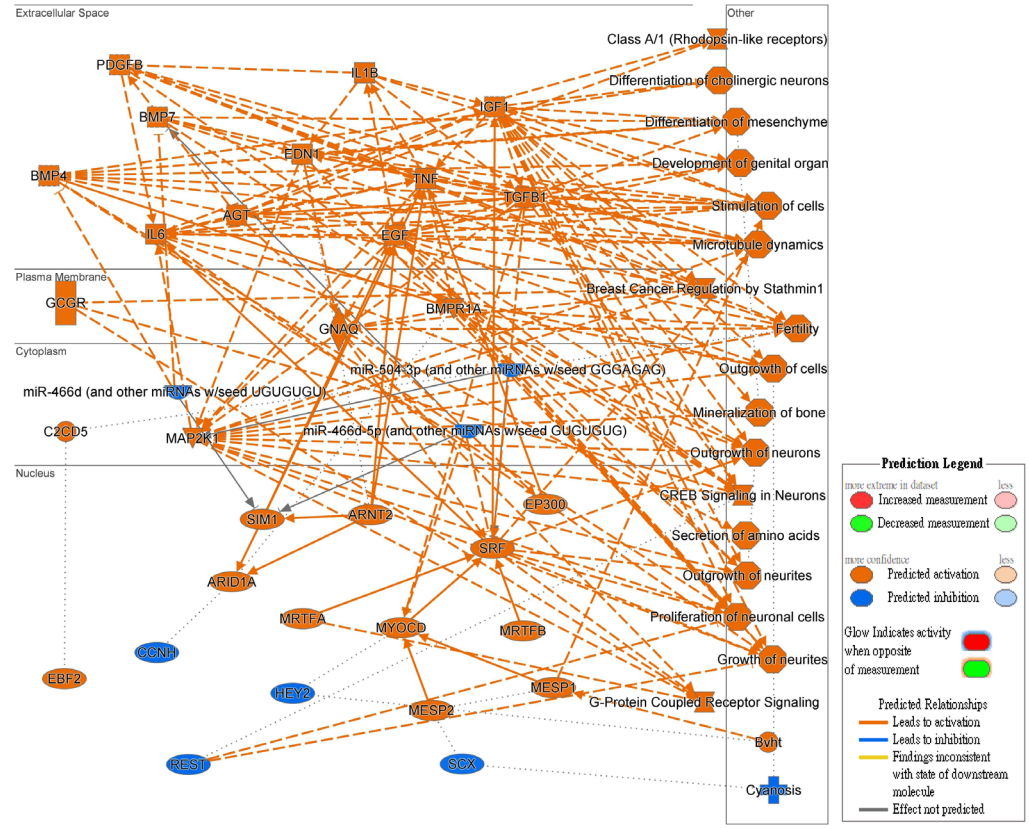
Extracellular Space
Other
Plasma Membrane
Cytoplasm
Nucleus
PDGFB
IL1B
IGF1
BMP7
EDN1
BMP4
TNF
TGFB1
AGT
IL6
EGF
GCGR
BMPR1A
GNAQ
C2CD5
MAP2K1
SIM1
ARNT2
EP300
SRF
ARID1A
MRTFA
MYOCD
MRTFB
CCNH
EBF2
HEY2
MESP1
MESP2
REST
SCX
Class A/1 (Rhodopsin-like receptors)
Differentiation of cholinergic neurons
Differentiation of mesenchyme
Development of genital organ
Stimulation of cells
Microtubule dynamics
Breast Cancer Regulation by Stathmin1
Fertility
Outgrowth of cells
Mineralization of bone
Outgrowth of neurons
CREB Signaling in Neurons
Secretion of amino acids
Outgrowth of neurites
Proliferation of neuronal cells
Growth of neurites
G-Protein Coupled Receptor Signaling
Bvht
Cyanosis
miR-504-3p (and other miRNAs w/seed GGGAGAG)
miR-466d (and other miRNAs w/seed UGUGUGU)
miR-466d-5p (and other miRNAs w/seed GUGUGUG)
Prediction Legend
more extreme in dataset
less
Increased measurement
Decreased measurement
more confidence
less
Predicted activation
Predicted inhibition
Glow Indicates activity when opposite of measurement
Predicted Relationships
Leads to activation
Leads to inhibition
Findings inconsistent with state of downstream molecule
Effect not predicted

B

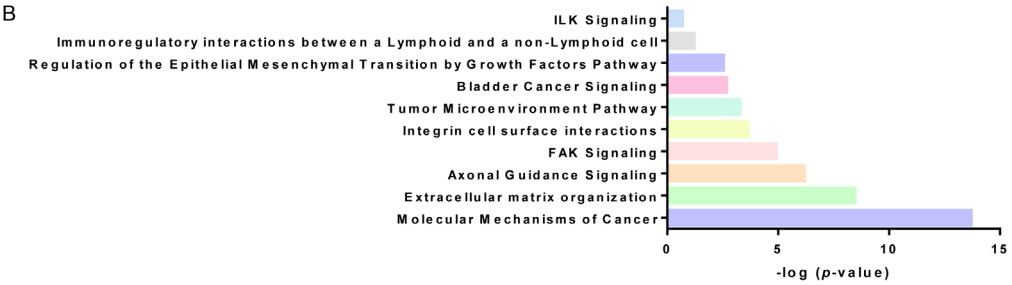
ILK Signaling
Immunoregulatory interactions between a Lymphoid and a non-Lymphoid cell
Regulation of the Epithelial Mesenchymal Transition by Growth Factors Pathway
Bladder Cancer Signaling
Tumor Microenvironment Pathway
Integrin cell surface interactions
FAK Signaling
Axonal Guidance Signaling
Extracellular matrix organization
Molecular Mechanisms of Cancer
0
5
10
15
-log (p-value)

C

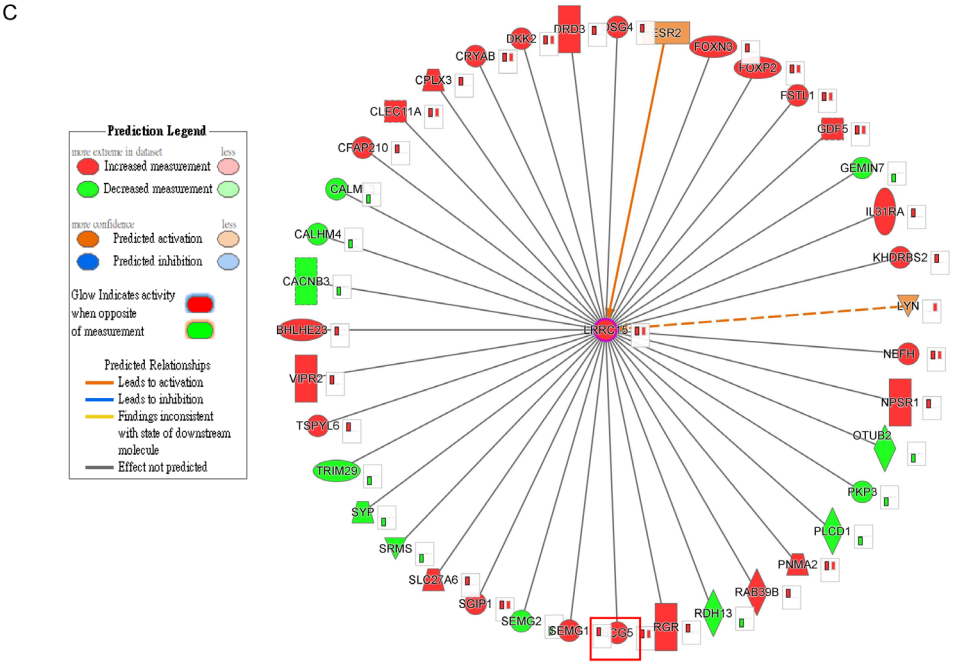
Prediction Legend
more extreme in dataset
less
Increased measurement
Decreased measurement
more confidence
less
Predicted activation
Predicted inhibition
Glow Indicates activity when opposite of measurement
Predicted Relationships
Leads to activation
Leads to inhibition
Findings inconsistent with state of downstream molecule
Effect not predicted
DKK2
DRD3
SG4
SR2
FOXN3
FOXP2
CRYAB
CPLX3
FSTL1
CLEC11A
GDF5
CFAP210
GEMIN7
CALM
IL31RA
CALHM4
KHDRBS2
CACNB3
LYN
BHLHE23
LRRC15
NEFH
VIPR2
NPSR1
TSPYL6
OTUB2
TRIM29
PKP3
SYP
PLCD1
SRMS
PNMA2
SLC27A6
RAB39B
SGIP1
RDH13
SEMG2
SEMG1
CG5
RGR

Supplementary Figure 3. Biological functions and molecular regulations of LRRC15 in upper tract urothelial carcinoma. A. Graphical summary profile illustrating the primary cellular functions associated with LRRC15 in UTUC. B. Gene Ontology analysis detailing the canonical pathways regulated by LRRC15 in UTUC. C. Molecular interaction map of LRRC15, depicting the affected molecules in UTUC.

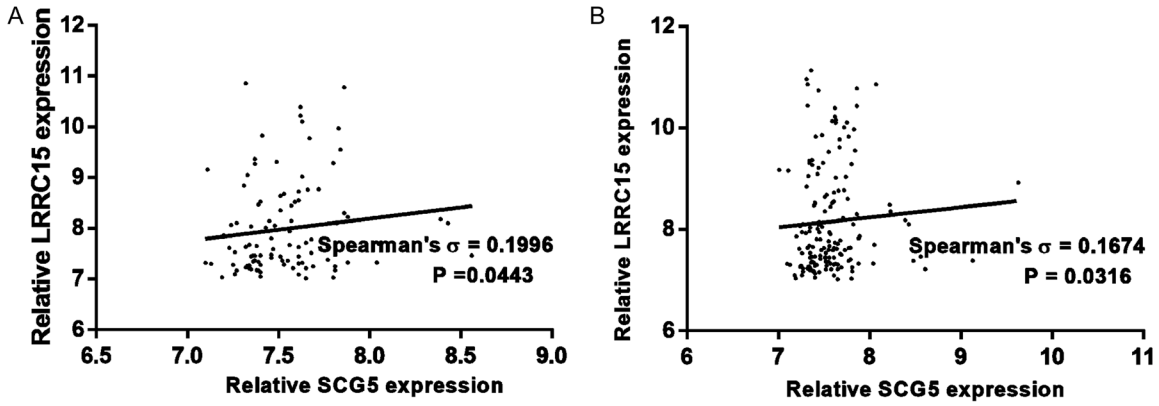

Supplementary Figure 4. Correlation of LRRC15 and SCG5 in non-muscle invasive bladder cancer and muscle invasive bladder cancer. A. Correlation between LRRC15 and SCG5 in NMIBC patients from the GSE13507 cohort. B. Correlation between LRRC15 and SCG5 in MIBC patients from the GSE13507 cohort.

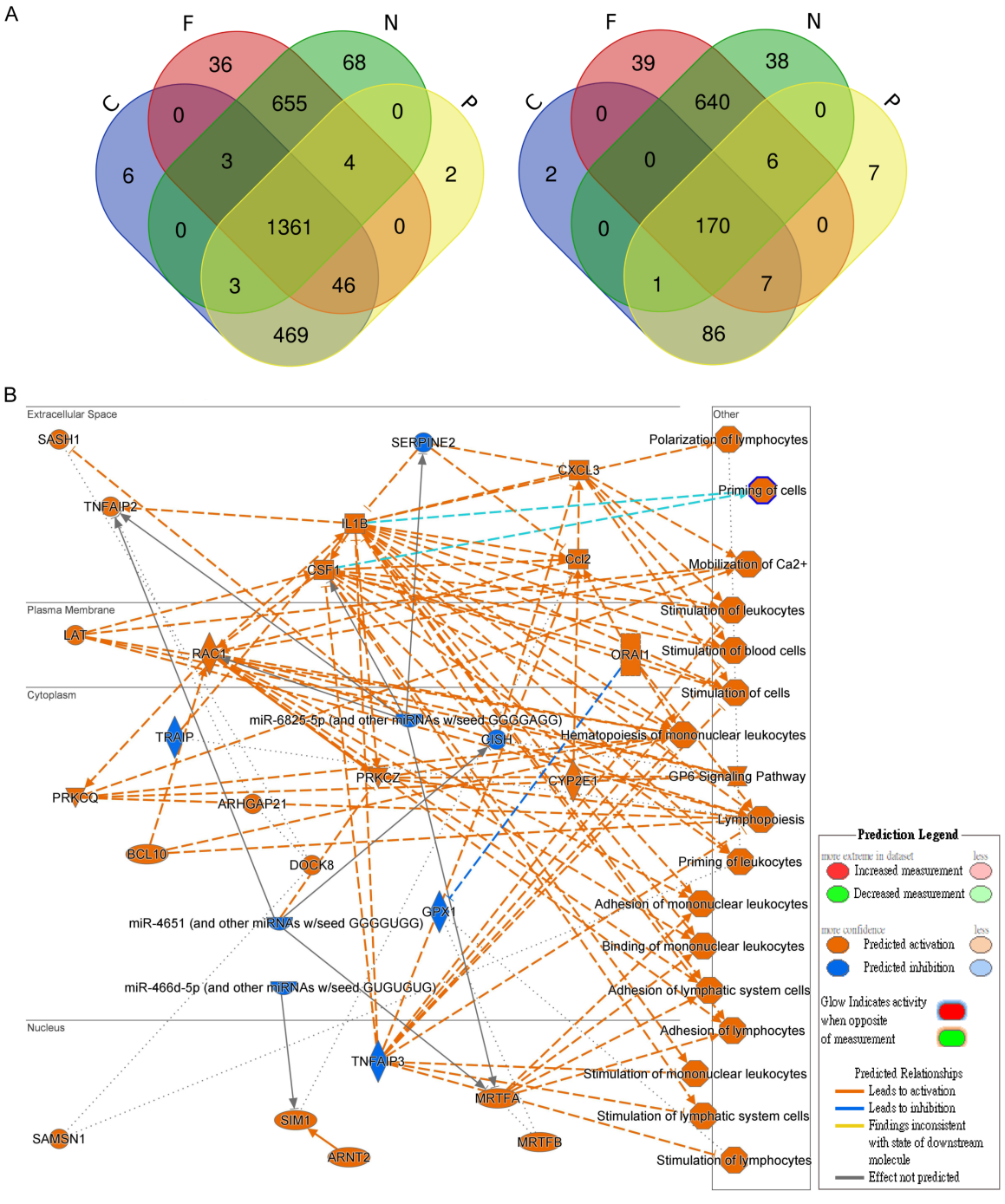
A
F
N
C
P
36
68
0
655
0
6
3
4
2
0
1361
0
3
46
469
F
N
C
P
39
38
0
640
0
2
0
6
7
0
170
0
1
7
86
B
Extracellular Space
Other
Plasma Membrane
Cytoplasm
Nucleus
SASH1
SERPINE2
CXCL3
Polarization of lymphocytes
Priming of cells
TNFAIP2
IL1B
Ccl2
CSF1
Mobilization of Ca2+
Stimulation of leukocytes
LAT
RAC1
ORAI1
Stimulation of blood cells
Stimulation of cells
miR-6825-5p (and other miRNAs w/seed GGGGAGG)
TRAIP
CISH
Hematopoiesis of mononuclear leukocytes
PRKCZ
CYP2E1
GP6 Signaling Pathway
PRKCQ
ARHGAP21
Lymphopoiesis
BCL10
DOCK8
Priming of leukocytes
GPX1
Adhesion of mononuclear leukocytes
miR-4651 (and other miRNAs w/seed GGGGUGG)
Binding of mononuclear leukocytes
miR-466d-5p (and other miRNAs w/seed GUGUGUG)
Adhesion of lymphatic system cells
Adhesion of lymphocytes
TNFAIP3
Stimulation of mononuclear leukocytes
MRTFA
Stimulation of lymphatic system cells
SIM1
SAMSN1
MRTFB
ARNT2
Stimulation of lymphocytes
Prediction Legend
more extreme in dataset
less
Increased measurement
Decreased measurement
more confidence
less
Predicted activation
Predicted inhibition
Glow Indicates activity when opposite of measurement
Predicted Relationships
Leads to activation
Leads to inhibition
Findings inconsistent with state of downstream molecule
Effect not predicted
C
Bladder Cancer Signaling
ILK Signaling
FAK Signaling
Regulation of the Epithelial Mesenchymal Transition by Growth Factors Pathway
Axonal Guidance Signaling
Tumor Microenvironment Pathway
Immunoregulatory interactions between a Lymphoid and a non-Lymphoid cell
Integrin cell surface interactions
Extracellular matrix organization
0
5
10
15
20
25
-log (p-value)

D

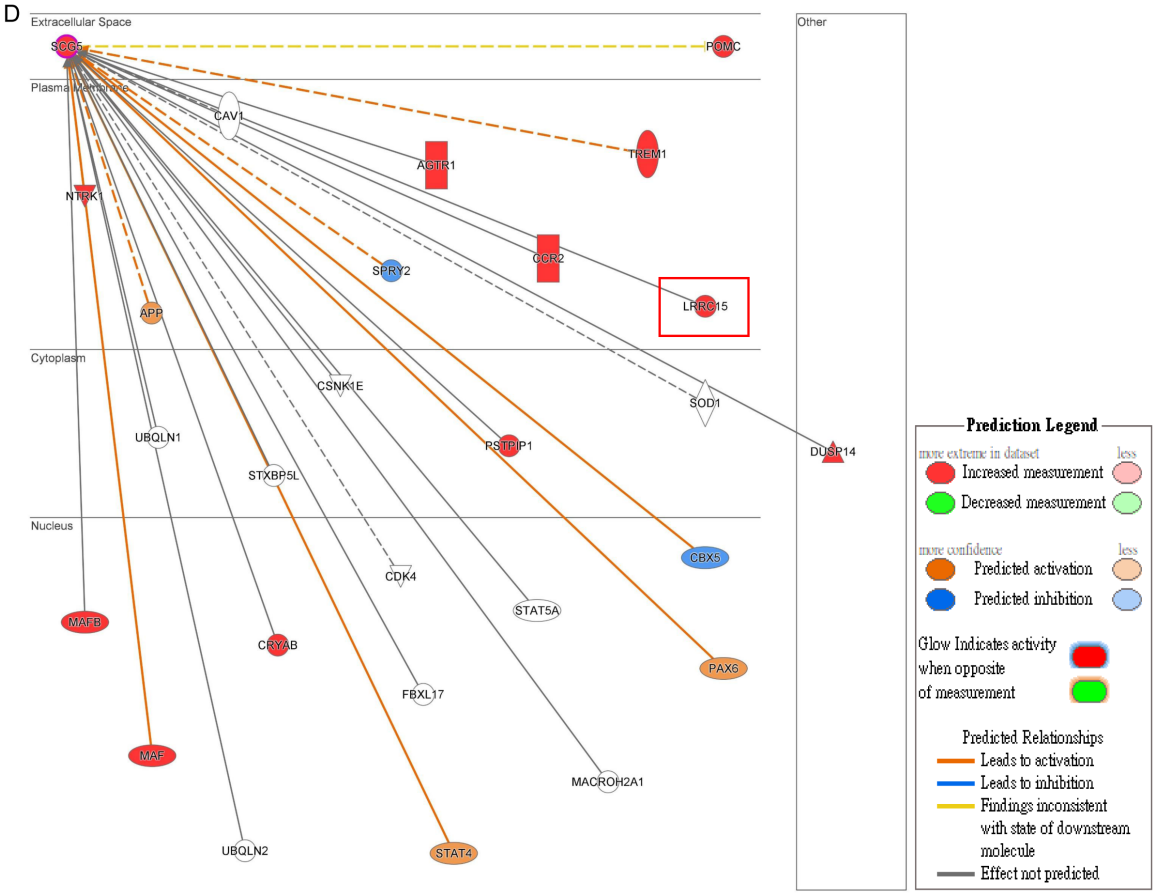

Supplementary Figure 5. Biological functions and molecular regulations of SCG5 in bladder cancer. A. Venn diagram illustrating the identification of molecules positively and negatively associated with SCG5 in bladder cancer. B. Graphical summary profile outlining the principal cellular functions associated with SCG5 in bladder cancer. C. Gene Ontology analysis listing the canonical pathways co-regulated by SCG5 in bladder cancer. D. Molecular interaction network of SCG5, showing the molecules impacted by SCG5 in bladder cancer.

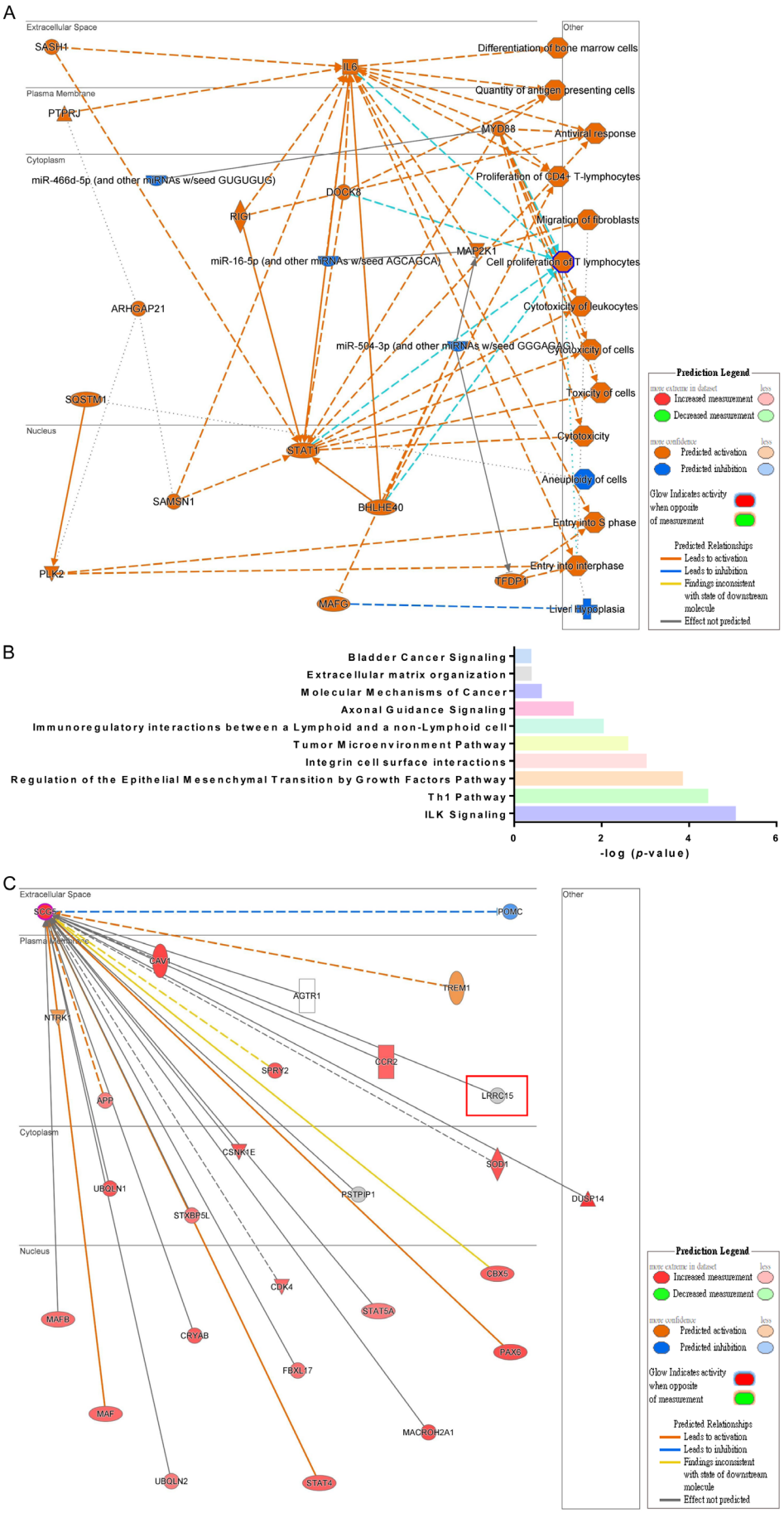
A
Extracellular Space
Plasma Membrane
Cytoplasm
Nucleus
Other
SASH1
IL6
PTPRJ
miR-466d-5p (and other miRNAs w/seed GUGUGUG)
DOCK8
RIGI
miR-16-5p (and other miRNAs w/seed AGCAGCA)
MAP2K1
ARHGAP21
SQSTM1
STAT1
SAMSN1
BHLHE40
PLK2
MAFG
TFDP1
miR-504-3p (and other miRNAs w/seed GGGACAG)
Differentiation of bone marrow cells
Quantity of antigen presenting cells
MYD88
Antiviral response
Proliferation of CD4+ T-lymphocytes
Migration of fibroblasts
Cell proliferation of T lymphocytes
Cytotoxicity of leukocytes
Cytotoxicity of cells
Toxicity of cells
Cytotoxicity
Aneuploidy of cells
Entry into S phase
Entry into interphase
Liver hyperplasia
Prediction Legend
more extreme in dataset
less
Increased measurement
Decreased measurement
more confidence
less
Predicted activation
Predicted inhibition
Glow Indicates activity when opposite of measurement
Predicted Relationships
Leads to activation
Leads to inhibition
Findings inconsistent with state of downstream molecule
Effect not predicted
B
Bladder Cancer Signaling
Extracellular matrix organization
Molecular Mechanisms of Cancer
Axonal Guidance Signaling
Immunoregulatory interactions between a Lymphoid and a non-Lymphoid cell
Tumor Microenvironment Pathway
Integrin cell surface interactions
Regulation of the Epithelial Mesenchymal Transition by Growth Factors Pathway
Th1 Pathway
ILK Signaling
0
2
4
6
-log (p-value)
C
Extracellular Space
Plasma Membrane
Cytoplasm
Nucleus
Other
SCG5
POMC
CAV1
AGTR1
TREM1
NTRK1
SPRY2
CCR2
LRRC15
APP
CSNK1E
SOD1
UBQLN1
PSTPIP1
DUSP14
STXBP5L
CBX5
CDK4
STAT5A
MAFB
CRYAB
PAX6
FBXL17
MAF
MACROH2A1
UBQLN2
STAT4
Prediction Legend
more extreme in dataset
less
Increased measurement
Decreased measurement
more confidence
less
Predicted activation
Predicted inhibition
Glow Indicates activity when opposite of measurement
Predicted Relationships
Leads to activation
Leads to inhibition
Findings inconsistent with state of downstream molecule
Effect not predicted

Supplementary Figure 6. Biological functions and molecular regulations of SCG5 in upper tract urothelial carcinoma. A. Graphical summary profile depicting the principal cellular functions associated with SCG5 in UTUC. B. Gene Ontology analysis detailing the canonical pathways co-regulated by SCG5 in UTUC. C. Molecular interaction network of SCG5, illustrating the molecules influenced by SCG5 in UTUC.

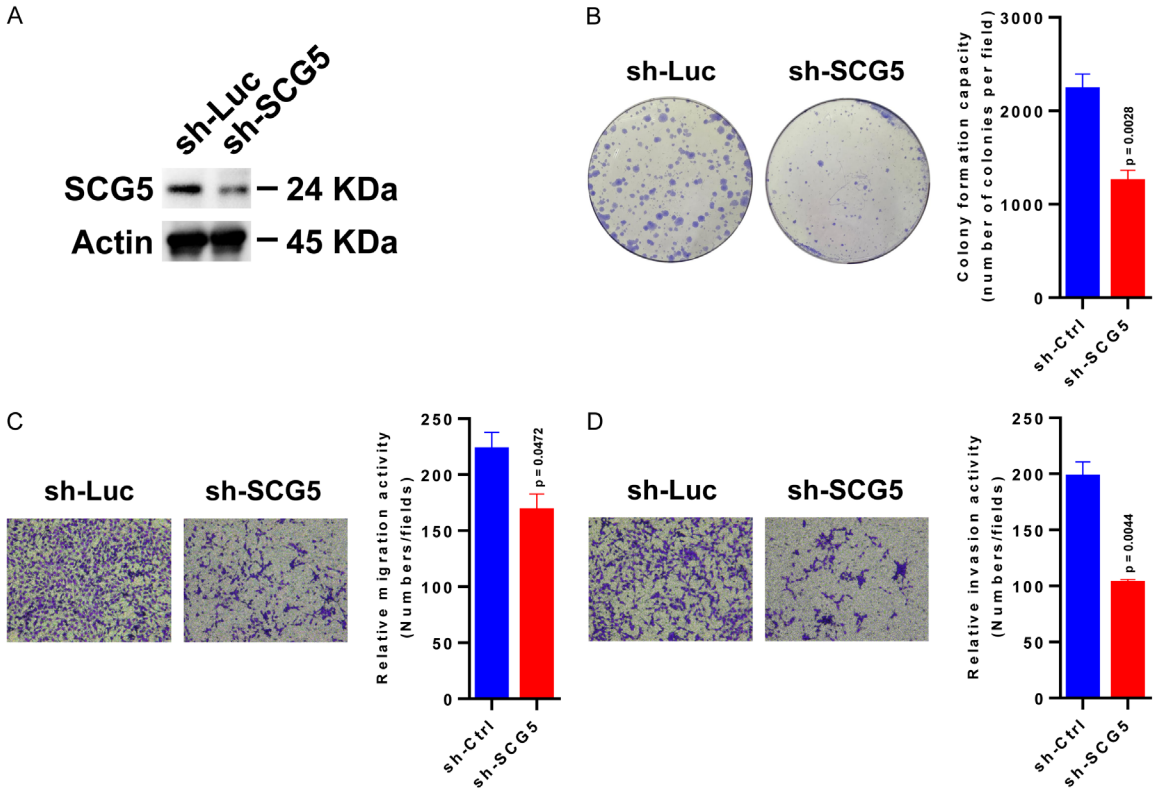

Supplementary Figure 7. Functional reprogramming of bladder cancer cells induced by SCG5 knockdown. A. Immunoblotting was utilized to verify the effective downregulation of SCG5 following lentiviral vector transduction. B. SCG5 depletion led to a significant reduction in the number and size of colonies formed by T24 cells. C. Silencing of SCG5 markedly impaired the directional motility of T24 bladder cancer cells in transwell-based migration settings. D. Invasion assays revealed that SCG5-deficient T24 cells exhibited markedly reduced capacity to penetrate Matrigel-coated membranes.

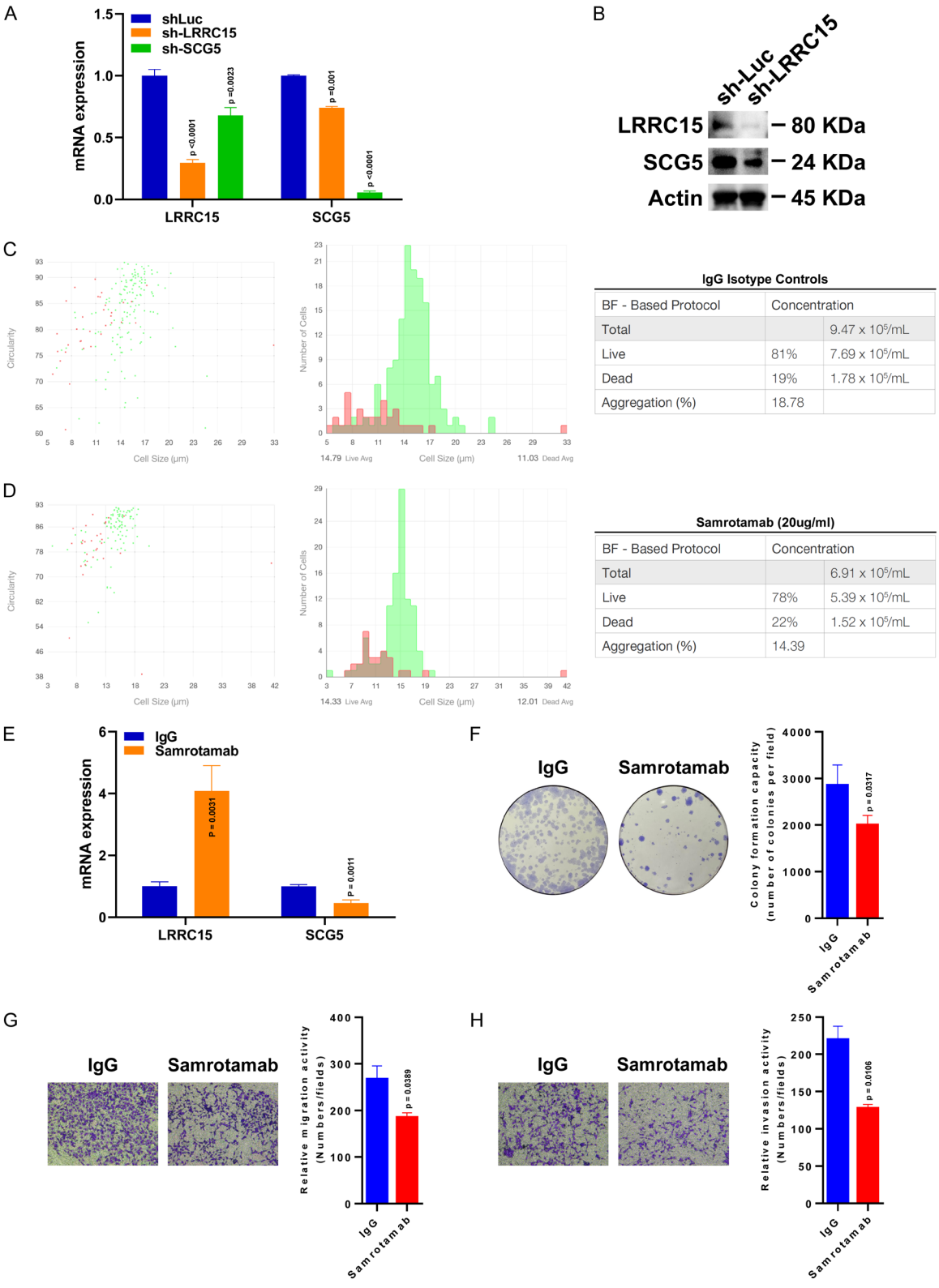

Supplementary Figure 8. Pharmacological or genetic blockade of LRRC15 and its downstream effector SCG5 suppressed key oncogenic hallmarks in bladder malignancy. A. The transcriptional consequences of LRRC15 or SCG5 knockdown were characterized by a comprehensive qPCR assessment of axis component expression. B. Western blot analysis revealed alterations in the expression patterns of LRRC15-SCG5 axis proteins following targeted gene silencing. C. The proliferative capacity of T24 tumor cells following a 24-hour exposure to 20 µg/mL IgG isotype con-

trol was quantified using the Countess 3 automated cell counter. D. T24 cell growth following a 24-hour treatment with Samrotamab at a concentration of 20 micrograms per milliliter was measured through Countess 3-based cell enumeration. E. The impact of Samrotamab-mediated LRRC15 inhibition on the LRRC15-SCG5 signaling axis in bladder cancer cells was quantitatively assessed by qPCR analysis. F. Exposure to Samrotamab caused a significant decline in colony formation by T24 cells. G. The migratory response of T24 cells under chemoattractant stimulation was notably suppressed by Samrotamab. H. The invasive capacity of bladder cancer cells was substantially reduced following Samrotamab treatment in chamber experiments.

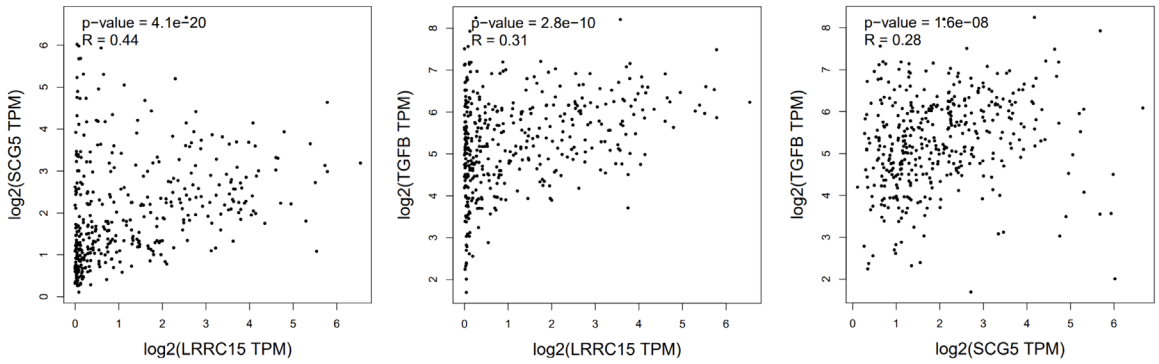

Supplementary Figure 9. Analysis of expression correlation and tissue distribution of LRRC15, SCG5, and TGF-β among TCGA bladder cancer patients.

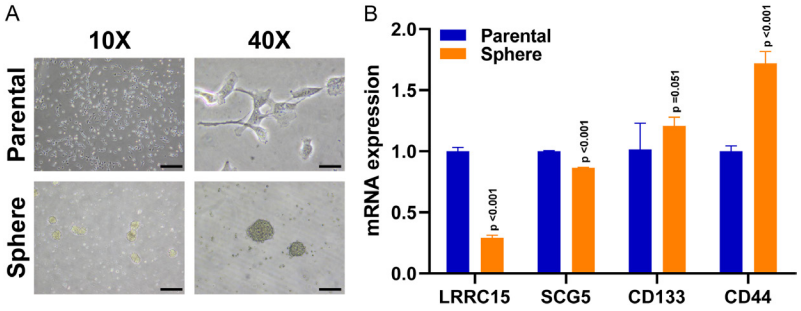

Supplementary Figure 10. Investigating the expression landscape of the LRRC15-SCG5 axis in bladder cancer stem cells. A. Representative micrographs at 10× and 40× magnifications illustrate the morphological characteristics of T24 cells cultured under adherent and ultra-low attachment conditions. B. The transcriptional activity of the LRRC15-SCG5 axis in stem-like bladder carcinoma cells was assessed using qPCR analysis.

Countess™ 3 Report

May 08, 2025 05:49 pm

Summary

Sample name: Countess
Count ID: 1006

Results

Trypan Blue corrected

BF - Based Protocol	Concentration	
Total		9.47 x 10^5/mL
Live	81%	7.69 x 10^5/mL
Dead	19%	1.78 x 10^5/mL
Aggregation (%)	18.78	

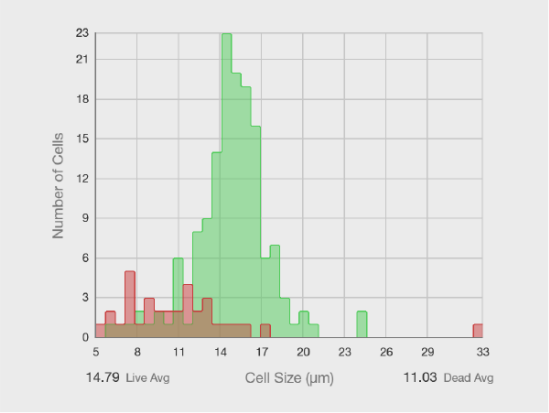

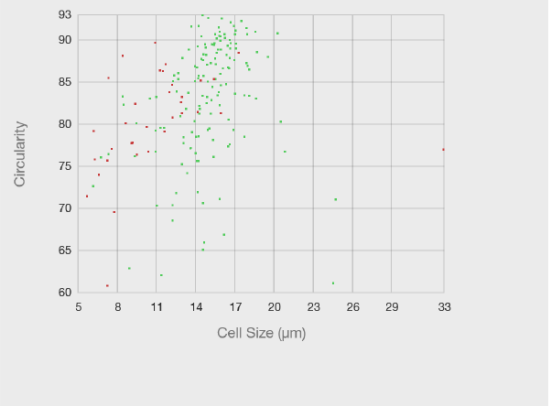

Settings

	Live	Dead	
Acquisition			
Intensity	39	39	
Focus	59	59	
Gating			
Protocol	Default Protocol		
Size	0, 70	0, 70	
Brightness	0, 255	0, 255	
Circularity	0, 100	0, 100	

Calculators

1:1 Trypan Blue:Sample

Countess™ 3
Automated Cell Counter

invitrogen
by Thermo Fisher Scientific

Countess™ 3 Report

Countess_BF

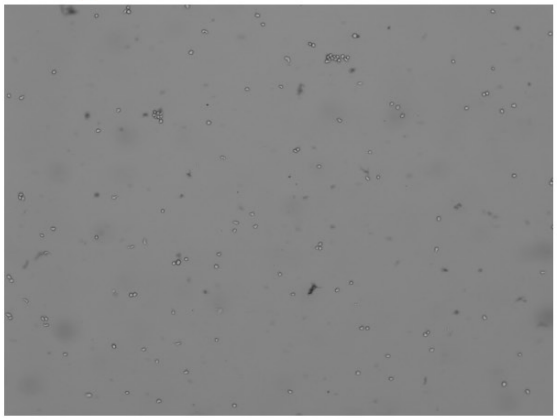

Countess

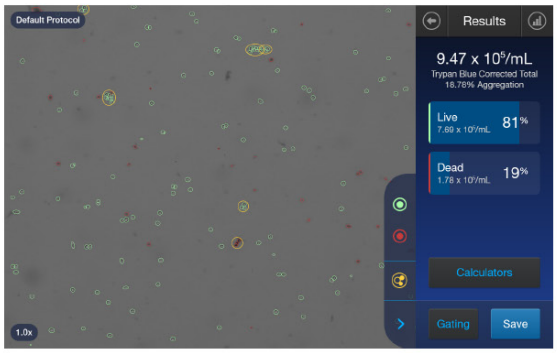

Countess™ 3
Automated Cell Counter

invitrogen
by Thermo Fisher Scientific

Countess™ 3 Report

May 08, 2025 05:51 pm

Summary

Sample name: Countess
Count ID: 1007

Results

Trypan Blue corrected

BF - Based Protocol	Concentration	
Total		6.91 x 10^5/mL
Live	78%	5.39 x 10^5/mL
Dead	22%	1.52 x 10^5/mL
Aggregation (%)	14.39	

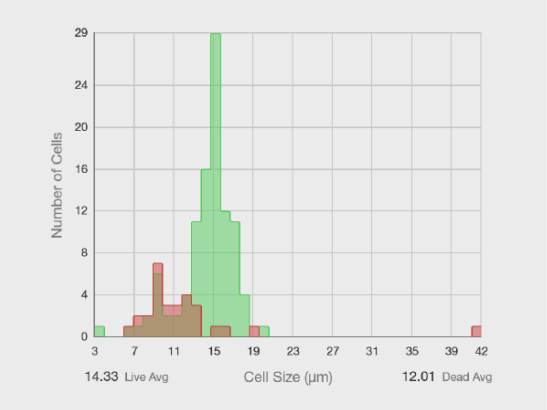

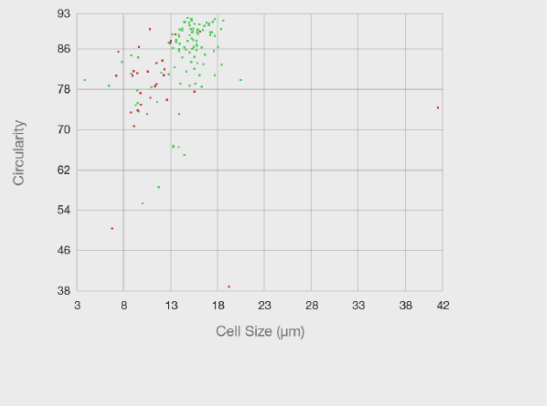

Settings

	Live	Dead	
Acquisition			
Intensity	39	39	
Focus	51	51	
Gating			
Protocol	Default Protocol		
Size	0, 70	0, 70	
Brightness	0, 255	0, 255	
Circularity	0, 100	0, 100	

Calculators

1:1 Trypan Blue:Sample

Countess™ 3
Automated Cell Counter

invitrogen
by Thermo Fisher Scientific

Countess™ 3 Report

Countess_BF

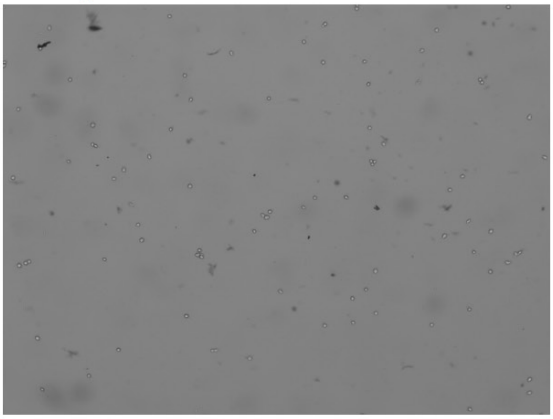

Countess

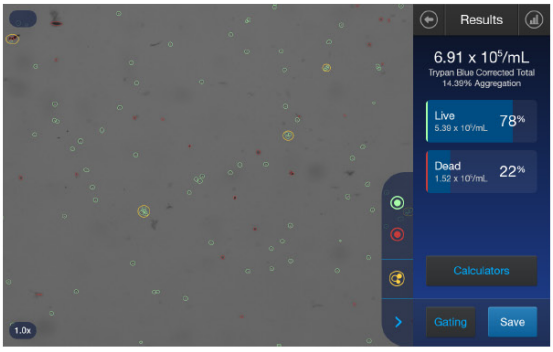

Countess™ 3
Automated Cell Counter

invitrogen
by Thermo Fisher Scientific

Supplementary Figure 11. Unprocessed quantitative datasets reflecting T24 cell viability post IgG and Samrotamab treatment were acquired using the Countess 3 cell analyzer.

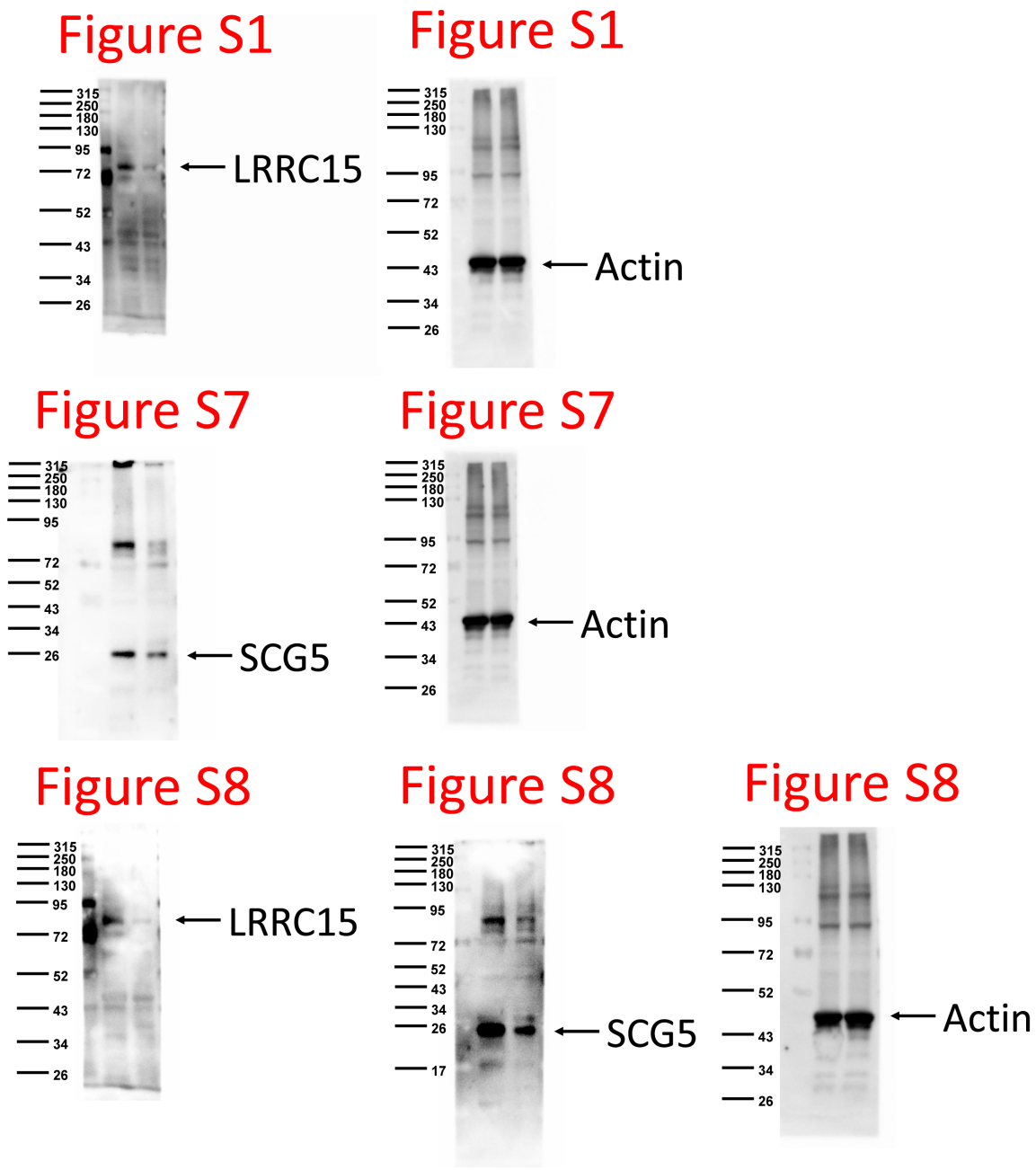

Supplementary Figure 12. The unprocessed immunoblot datasets supporting this analysis are available.